

**VIBRATION ANALYSIS OF COMPOSITE LAMINATED SHELLS
USING 2D SPECTRAL CHEBYSHEV METHOD AND
LAMINATION PARAMETERS**

by
PEIMAN KHANDAR SHAHABAD

Submitted to the Graduate School of Engineering and Natural Sciences
in partial fulfilment of
the requirements for the degree of Master of Science

Sabanci University
July 2021

**VIBRATION ANALYSIS OF COMPOSITE LAMINATED SHELLS
USING 2D SPECTRAL CHEBYSHEV METHOD AND
LAMINATION PARAMETERS**

Approved by:

[Redacted signature]

[Redacted signature]

[Redacted signature]

Date of Approval: July 12, 2021

THESIS AUTHOR 2021 ©

All Rights Reserved

ABSTRACT

VIBRATION ANALYSIS OF COMPOSITE LAMINATED SHELLS USING 2D SPECTRAL CHEBYSHEV METHOD AND LAMINATION PARAMETERS

PEIMAN KHANDAR SHAHABAD

Mechatronics Engineering

M.S. THESIS, July 2021

Thesis Supervisor: Assist. Prof. Bekir Bediz

Keywords: Vibration analysis, laminated composites, sandwich plates, conical shells, lamination parameters, spectral Chebyshev, optimization; layup optimization

This study presents a modeling approach to accurately and efficiently predict the dynamics of laminated composite structures. The governing equations are derived based on the first order shear deformation theory kinematic equations following the Hamilton's principle. To express the strain energy of the shells, in-plane and bending lamination parameters are used. A two-dimensional spectral approach based on Chebyshev polynomials is implemented to solve the governing equations. The developed framework including the spectral Chebyshev approach and lamination parameters results in an accurate and computationally efficient solution method. To demonstrate the performance of the presented solution approach, various case studies including straight panels, curved shells, truncated conical shells, and sandwich panels are investigated. The benchmarks indicate that the calculated non-dimensional natural frequencies and critical buckling loads excellently match the results found using finite element method and the simulation duration can be decreased by 100 folds. To leverage the computational performance of the presented approach, a stacking sequence optimization is performed to maximize the fundamental frequency of a shell geometry, and the corresponding fiber angles are retrieved from the optimized lamination parameters. Furthermore, a parametric analysis is performed to investigate the effect of geometry on the optimized lamination parameters (and fiber angles) based on fundamental natural frequency maximization.

ÖZET

2B SPEKTRAL CHEBYSHEV YÖNTEMİ VE LAMINASYON PARAMETRELERİ KULLANILARAK KOMPOZİT KABUKLARIN TİTREŞİM ANALİZİ

PEİMAN KHANDAR SHAHABAD

Mekatronik mühendisliği
YÜKSEK LİSANS TEZİ, Temmuz 2021

Tez Danışmanı: Assist. Prof. Bekir Bediz

Anahtar Kelimeler: titreşim analizi, Katmanlı kompozitler, sandviç plakalar, konik kabuklar, laminasyon parameterleri, spektral-Chebyshev, eniyileme, yerleştirme optimizasyonu

Bu çalışma, katmanlı kompozit yapıların dinamiklerini doğru ve verimli bir şekilde tahmin etmek için bir modelleme yöntemi sunmaktadır. Hareket denklemleri, birinci dereceden kayma deformasyon teorisi kinematik denklemleri ve Hamilton ilkesi kullanılarak elde edilmiştir. Enerji tabanlı bu yöntemde, yapının gerinim enerjisini ifade etmek için düzlem içi ve eğilme laminasyon parametrelerinden faydalanılmıştır. Hareket denklemini çözmek için Chebyshev polinomlarına dayalı iki boyutlu bir spektral yaklaşım geliştirilmiştir. Geliştirilen yöntemin performans analizi için düz paneller, kavisli kabuklar, kesik konik kabuklar ve sandviç paneller dahil olmak üzere çeşitli çalışmaları incelenmiştir. Yöntemin doğruluğunun tespiti için doğal frekans ve kritik burkulma yükleri sonlu elemanlar yöntemi ile bulunanlarla karşılaştırılmıştır. Karşılaştırmalar sonucu aynı hassasiyetteki sonuçların en az 100 kat daha hızlı elde edilebildiği gözlemlenmiştir. Sunulan çözüm yönteminin hesaplama performansından yararlanmak için, bir kabuk geometrisinin temel frekansını en üst düzeye çıkarmak için bir istifleme dizisi eniyilemesi (optimizasyonu) gerçekleştirilmiştir. Bunun optimum konfigürasyona (optimize edilmiş laminasyon parametrelerine) karşılık gelen fiber açıları bulunmuştur. Ayrıca, temel doğal frekans maksimizasyonuna dayalı olarak optimize edilmiş laminasyon parametreleri (ve fiber açıları) üzerinde geometrinin etkisini araştırmak için bir parametrik analiz yapılmıştır.

ACKNOWLEDGEMENTS

I would like to thank, first and foremost, to my advisor Dr. Bekir Bediz for his guidance, patience and endless support during my M.Sc. study. I am really thankful that I found the opportunity to benefit from his experiences that helped me to develop myself in science and research. I am always consider my self fortunate to be a member of his research team.

My appreciations goes to Prof. Ipek Başdoğan and Prof. Güllü Kızıldağ şundur along with my thesis committee members for agreeing to join my thesis defense jury. I want to express my gratitude for their valuable knowledge and comments which assisted me to complete my thesis .

I would like to acknowledge Scientific and Technological Research Council of Turkey (TUBITAK) in which supports this research under Grant No. 120M598. (PI: Bekir Bediz)

I would like thank Sabanci University, Engineering and natural science faculty, and Mechatronics group for providing an exceptional and convenient educational and research environment for the graduate students. I would like to thank Mirmeysam Rafiei Anamagh for his useful advises, contributions and motivation in last two years. He was not only a colleague , he was a friend and supporter and a person who was always there whenever I needed.

I wanna express my gratitude to Dr. saeed lotfan and Dr. Gökhan serhat for their collaboration and innovative ideas during my M.Sc and also I want to thank Farzad Seyyed Rahmani.

I thank to my teammates Kazi Sher Ahmad and Andisheh Chopani for their motivational talks and positive vibes during my courses in graduate study. Also thanks to my lab mates Ender Eđer and Ece Kurt for good memories during my master years

Also, I thank to all my friends in Iran, Turkey and all around the world who always stay beside me throughout my life.

I would like to thank my beloved family for all the inspiration, unconditional support throughout my lifetime. They have always encouraged me to follow my dreams. Without their support, guidance, and encouragement this thesis would not have been possible.

I dedicate my thesis

In memory of my grandmother Parijun I will never forget her.

My beloved sister Negar who always stands by me when things look bleak.

And my mother and father for their sincere and unconditional love and ever-present supports.

I will always love you

TABLE OF CONTENTS

LIST OF TABLES	x
LIST OF FIGURES	xii
1. Introduction	1
1.1. Composite Materials	1
1.1.1. Classification of composite materials	2
1.1.1.1. Laminated composite structures	5
1.1.1.2. Sandwich composite structures	6
1.1.2. Applications of composite materials	6
1.2. Modeling of Composite Structures	7
1.2.1. Classical laminated plate deformation theory (CLPT)	8
1.2.2. First-order shear deformation theory (FSDT)	9
1.2.3. Higher-order shear deformation theory (HSDT)	10
1.3. Solution Methods	11
1.4. Design of Composite Structures	13
1.5. Thesis Objective	14
1.6. Research Contribution	15
1.7. Thesis Outline	16
2. Problem Description	17
2.1. Laminated Panels and Shells	17
2.1.1. Stiffness formulation using lamination parameters	18
2.1.2. Derivation of the boundary value problem	23
2.2. Spectral Chebyshev Approach	24
3. Model Validation and Results	32
3.1. Laminated Composite Structures	33
3.1.1. Case study I: Straight panel	33
3.1.1.1. Modal Analysis	34
3.1.1.2. Buckling analysis	37

3.1.2. Case study II: Cylindrical shell	38
3.1.3. Case study III: Conical shell	40
3.2. Sandwich Structures	42
3.2.1. Modal Analysis.....	42
3.2.2. Buckling analysis	43
4. Design of Laminated Composite Panels	47
4.1. Fundamental Frequency Maximization	47
4.2. Effect of Geometry on Fundamental Frequency Maximization	49
5. Conclusion	52
6. Future Work.....	54
BIBLIOGRAPHY.....	55

LIST OF TABLES

Table 3.1. Material properties of the unidirectional lamina.....	32
Table 3.2. Material properties of the unidirectional laminae.	33
Table 3.3. Convergence of the first ten (non-dimensional) natural frequencies for a straight laminated composite panel having a geometry of $L_y/L_x = 1$ and $h/L_x = 0.05$, and a layup of $[45/0]_s$ under $SSSS$ boundary condition.	35
Table 3.4. Polynomial numbers (N_x-N_s) used in the validation studies based on the convergence analyses.	36
Table 3.5. Comparison of the first ten (non-dimensional) natural frequencies of straight composite laminated panels having different aspect ratios and symmetric layup configurations under $SSSS$ and $CCCC$ boundary conditions.	37
Table 3.6. Comparison of the required DOFs and the computational cost of validation case studies in Table 3.5.....	37
Table 3.7. Comparison of the (non-dimensional) critical buckling load of straight composite laminated panels having different aspect ratios and symmetric layup configurations under $SSSS$ boundary condition.	39
Table 3.8. Polynomial numbers (N_x-N_s) used in the validation studies of cylindrical shells based on the convergence analyses.	39
Table 3.9. Comparison of the first ten (non-dimensional) natural frequencies of cylindrical composite laminated panels having different curvature amounts and symmetric layup configurations under $SSSS$ and $CCCC$ boundary conditions.	40
Table 3.10. Polynomial numbers (N_x-N_s) used in the validation studies of truncated conical shells based on the convergence analyses.	41
Table 3.11. Comparison of the first ten (non-dimensional) natural frequencies of truncated conical composite laminated panels having different apex angles and symmetric layup configurations under $CCCC$ and $SSSS$ boundary conditions.	41

Table 3.12. Polynomial numbers (N_x-N_s) used in the validation studies of laminated sandwich panels based on the convergence analyses	43
Table 3.13. Comparison of the first five (non-dimensional) natural frequencies of straight laminated sandwich panels having different aspect ratios and symmetric layup configurations under <i>SSSS</i> and <i>CCCC</i> boundary conditions.	43
Table 3.14. Comparison of the required DOFs and the computational cost of validation case studies in Table 3.13.	44
Table 3.15. Comparison of the (non-dimensional) critical buckling load of straight laminated sandwich panels having different aspect ratios and symmetric layup configurations under <i>SSSS</i> boundary condition.	44
Table 4.1. Optimized lamination parameters and the corresponding fiber angles and stacking sequence of laminated conical shell under <i>CSCS</i> boundary conditions that maximizes non-dimensional fundamental frequency.	49
Table 4.2. Optimal layups considering 15° and 1° angle increments.	49
Table 4.3. Optimal layups considering 12 layers and 15° angle increments for the selected geometries shown by the dashed red curves in Figs. 4.2 and 4.3.	51

LIST OF FIGURES

Figure 1.1. Schematic of a composite material.	2
Figure 1.2. Schematic of particulate and flake composites	3
Figure 1.3. Fiber arrangement patterns in a composite layer	4
Figure 1.4. (a) A traditional composite- (b) functionally graded material .	5
Figure 1.5. Cross-section of undeformed and deformed geometries of a plate based on CLPT	8
Figure 1.6. Cross-section of undeformed and deformed geometries of a plate based on FSDT	9
Figure 1.7. Cross-section of undeformed and deformed geometries of a plate based on HSDT	10
Figure 2.1. Schematics of (a) a general curved conical panel geometry and (b) cross-section view of the laminated shell.	18
Figure 2.2. cross-section view of the half laminated sandwich shell	20
Figure 3.1. Schematics of a laminated straight panel	34
Figure 3.2. Stacking sequence of laminated composite with $[45/0]_s$ layup .	34
Figure 3.3. Convergence contour plots for the validation of straight panels having $L_y/L_x = 1, 1.5, \text{ and } 2$ under $SSSS$ boundary condition	36
Figure 3.4. Load types in straight laminated composites. Red arrows im- ply uni-axial loading, and red and blue lines imply bi-axial loading. ...	38
Figure 3.5. Convergence contour plots for the validation of cylindrical shells having $\Theta = 45^\circ, 60^\circ, \text{ and } 120^\circ$ under $SSSS$ boundary condition	40
Figure 3.6. Convergence contour plots for the validation of truncated con- ical panel having $\alpha = 30^\circ, 45^\circ, \text{ and } 60^\circ$ under $SSSS$ boundary condition	41
Figure 3.7. Effects of aspect ratios L_y/L_x on non-dimensional critical buckling load under uni-axial (a) and bi-axial (b) buckling forces for uniform layer thickness sandwich	45
Figure 3.8. Effects of aspect ratios L_y/L_x on non-dimensional critical buckling load under uni-axial (a) and bi-axial (b) buckling forces for variable layer thicknesses sandwich $[(90/\pm 45/0)/(90/0)_2]_s$ layup	45

Figure 4.1. 8-layered laminated truncated conical shell with $\alpha = 60^\circ$, $L_s/L_x = 2\pi/3$, $h/L_x = 0.05$ and $R_1/L_x = 0.5$ geometry properties	48
Figure 4.2. Effect of curvature amount (Θ) on maximized natural frequency, $(\bar{\omega}_o)_{\max}$, of a conical panel having $L_s/L_x = \pi/4$ and $h/L_x = 0.05$ under (a) <i>SSSS</i> and (b) <i>CCCC</i> boundary conditions for various semi-vertex angle. Blue, red, green, and black lines represent the semi-vertex angles of 15° , 30° , 45° , and 60° , respectively.	50
Figure 4.3. Effect of semi-vertex angle (α) on maximized natural frequency, $(\bar{\omega}_o)_{\max}$, of a conical panel having $L_s/L_x = \pi/4$ and $h/L_x = 0.05$ under (a) <i>SSSS</i> and (b) <i>CCCC</i> boundary conditions. Blue, red, green, black, and magenta lines represent the curvature amount of 30° , 45° , 60° , 90° , and 120° , respectively.	50

1. Introduction

Materials and structures always play an essential role in human beings and civilization. In recent years, material science has achieved rapid developments, mainly due to the increased interdisciplinary research. The main motivation is that new material developments lead to novel advanced materials and applications. Composite materials represent nothing but a giant step in terms of the efficient use and innovation of materials [1,2]. By significant developments in composite materials and their manufacturing process, it has drawn quite a lot of attention. Recently, conventional composites have been shifting towards advanced composite materials [3,4].

Composite materials are mainly designed and fabricated in the form of beams, shells, and plates. Due to the high number of applications in various fields of engineering (such as aerospace, automotive, and energy fields), there is a growing demand to understand the static/dynamic behavior of (laminated) plate/shell composite structures.

This chapter presents an overview of composite materials, mainly modeling the dynamic behavior of laminated composite structures. Therefore, initially a brief definition and classification of composite structures are presented. Next, different modeling approaches to approximate the kinematics and numerical methods to analyze the governing equation of the composite plates have been discussed. Then, a detailed literature review about layup optimization of laminated composite shells and plates is presented. Later, the aim of this study is highlighted.

1.1 Composite Materials

Composite materials are made up of two or more materials on a macroscopic scale that provides desirable properties. These superior properties cannot be attained by any of the constituents alone. The combination of components results in two phases:

(i) reinforcement and (ii) matrix (see Fig. 1.1). Reinforcement is a discontinuous phase and generally strong. In addition, due to high stiffness properties, reinforcement is a bearing phase when an external load is applied to the structure. On the other hand, the matrix is a continuous phase that holds the reinforcements together. The most outstanding advantages that enhance the use of composite materials are low density, high stiffness and strength, long fatigue life, remarkable life cycle cost, and low thermal expansion. In addition, due to the variety of combinations of reinforcement and matrix materials, designers have great opportunities to tailor the design to achieve better performance in terms of application and resources [5–8].

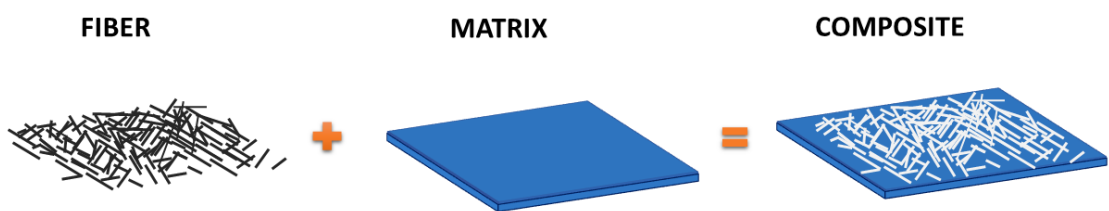


Figure 1.1 Schematic of a composite material.

1.1.1 Classification of composite materials

Generally, composite materials are classified based on the matrix material and the shape and size of the reinforcement. According to the type of matrix materials, they can be categorized into three sections:

- metal matrix composite
- resin matrix composite
- ceramic matrix composite

According to the shape and size of reinforcement, composites can be divided into five main groups:

- Particulate composites
- Flake composites
- Fiber-reinforced composites
- Functionally graded composites

- Layered composites

Particulate composites consist of dispersed stiff constituents in a softer matrix material (see Fig. 1.2a) [7, 9]. The material used in reinforcement of particulate composites can be either metallic or non-metallic. One of the well-known particulate composites is concrete, in which gravel and cement are reinforcement and matrix, respectively.

Flake composite, as its name signifies, is made up of thin flakes in a matrix (see Fig. 1.2b) [7, 10]. Flake composite formed a more orderly configuration/distribution than particulate composites, and therefore, the material properties can be more uniform in a plane. Common examples of flake materials are glass, metals, carbon, and mica. However, the size and shape of the utilized flake depend on the type of application. Matrix material for such structures can be either plastic, metal, or epoxy resin.

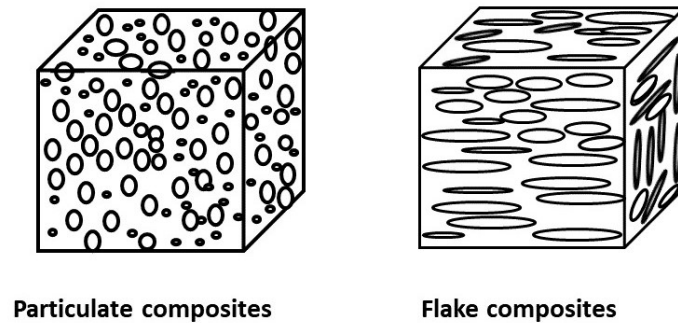


Figure 1.2 Schematic of particulate and flake composites

Fiber-reinforced composites are the most commonly used composite structures and are made up of reinforcing agents such as glass fiber, carbon fiber, or boron fiber. The matrix part can be considered as resin, plastic, rubber, or metal. Since fibers in such structures are generally stiff and strong, they play a crucial role as a load-carrying constituent. In addition, the matrix part holds the fibers together and distributes the applied load. Furthermore, fiber-induced composites can be tailored easily by changing the orientation of fibers.

As shown in Fig. 1.3, fiber-reinforced composites can be categorized based on the dimension and distribution of fibers. For example, according to the length of fibers they can be considered as short or continuous fibers while due to distribution they can be randomly dispersed, oriented, or in the weave form. Among the mentioned groups, continuous fibers are the most common type. Continuous fiber is geometrically characterized as having a very high length to diameter ratio. In addition, it's

high strength and modulus features make them more valuable. Uni-directional, bi-directional and randomly distributed fiber-reinforced composites can be considered as common configuration of continuous fiber composites.

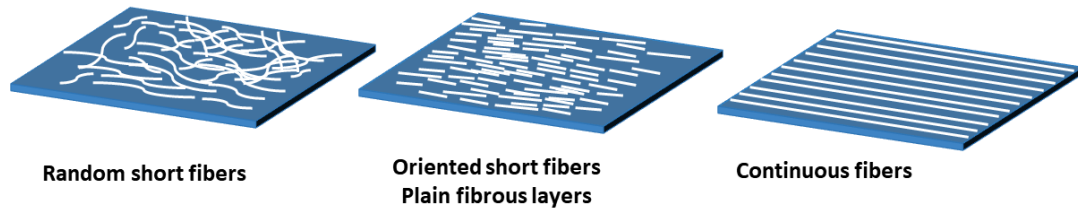
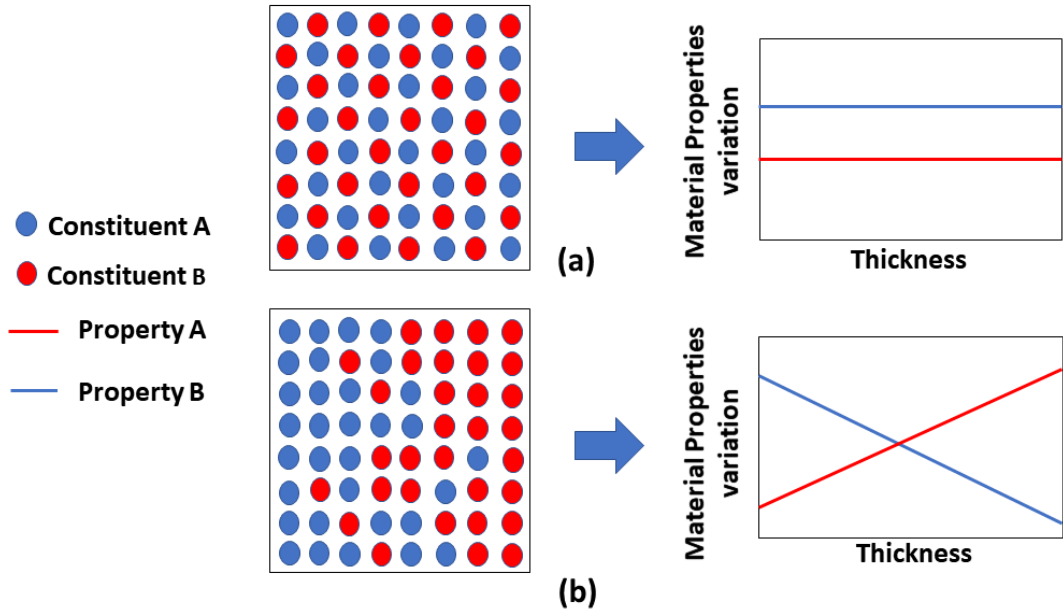


Figure 1.3 Fiber arrangement patterns in a composite layer

Functionally graded materials (FGM) are characterized by the compositional gradient of one material into another across the volume (along one or more directions) which is illustrated in Fig 1.4. The overall properties of FGM are unique and different from their homogeneous counterparts. The main advantage of FGM is combining the best properties of both materials and provides a smooth transition of material properties. For example, in metal-ceramic reinforced-based FGMs, the ceramic part can resist against high temperature. At the same time, the metallic material can provide mechanical properties of structure in order to support ceramic parts. As it seen from Fig 1.4, gradual variation of material properties eliminates the sharp interface between the constituent materials. Therefore, the stress concentration and delamination will be decreased.

Commonly, FGMs can be divided into three main categories: chemical composition gradient, porosity gradient, and microstructure gradient. FGMs have the potential to be used in a wide range of fields such such as aerospace, biomaterials, biomedical, etc. [11–14].



The last type of composite structures is the layered composite materials which consist of well-bonded several thin layers together. In that case, the material properties of each layer can be identical or different with each other based on the type of composite. According to that, they can be divided into two main categories as laminated composite structures and sandwich composite structures [5, 7, 9, 11].

1.1.1.1 Laminated composite structures

A *lamina* or *ply* is referred to as a typical sheet of composite material which involves fibers with the same orientation. A laminated structure is a collection of stacked laminae to achieve desired stiffness and strength. For instance, unidirectional fiber-reinforced lamina can be stacked so that the fibers in each lamina are oriented in the same or different orientations. The sequence of various directions of a fiber-reinforced composite layer in a laminate is termed *the stacking sequence*.

Laminated composite structures, which are generally in the shape of beams, shells, or plates, are widely adopted in various engineering applications such as aerospace and automobile industries. The mechanical properties of these structures predominantly depend on stacking sequences, fiber orientations, and ply thicknesses. Thus, proper tailoring of laminate configuration can improve strength and stiffness-to-weight ratios effectively [8, 9].

1.1.1.2 Sandwich composite structures

Sandwich composite structures are a particular type of layered composites characterized by a combination of different materials bonded together to cooperate with their single properties to the global structure's performance. The sandwich structure is divided into three main parts: two external thin and stiff face sheets, and a thick and soft core. The materials in face sheets and core can be fiber-reinforced and/or FGM [4, 15–19].

The primary motivation behind sandwich structures and replacing them with conventional composites is hybridization. Hybridization is an effective method in which a high-stiffness and more expensive material (e.g., Graphite/epoxy) is used in the outer layers and inexpensive low-stiffness material in the inner layers (e.g., Glass/epoxy) [20]. This concept provides a suitable structural rigidity and a significant cost reduction [20–22]. Despite the advantages of sandwich structures, their analysis and design become challenging due to the considerable variation of material properties between the core and the face sheets. Hence, proper optimization procedure in such structures plays a crucial role as well as laminated composites [20, 23–25].

1.1.2 Applications of composite materials

The use of composite materials traced back thousands of years ago. In 4000 B.C., papyrus plants were used as fibrous composite materials to make laminated writing materials. In addition, ancient civilizations used straw as reinforcement for making mud bricks [2, 7]. Also, the potential of forming glass fibers was considered by scientists in the 18th century [2]. Although man-made composites have existed for many years, composite technology has evolved in the last fifty years.

The developments in materials science and manufacturing processes lead to outstanding improvements in applications of composite structures, particularly in aerospace structures and athletic equipment. Furthermore, applications in the infrastructure and automobile industry, which used all-composite structures, can be considered as other examples of composite usage. As the technology grows, new/novel composites and technologies are being developed and adapted, such as composites with structure–function integration, functional and multifunctional composites, intelligent composites and nanocomposites [4].

Due to the anisotropic nature and various applications of layered composite mate-

rials, studies involving the stability behaviors and natural vibrations of those structures to predict their structural responses become a significant issue. Therefore, achieving the best possible structural performance requires accurate modeling of the physical properties and optimization of the design parameters. However, due to the high number of design parameters, an accurate and computationally efficient modeling approach is direly required to achieve an optimized and reliable design for the desired application.

1.2 Modeling of Composite Structures

The fiber-reinforced laminated composite structures, unlike their isotropic counterparts, lead to significant challenges in the modeling process due to the interfaces between layers and mismatch of material properties [9]. Moreover, to define the deformation of laminated composite structures, complex couplings between extension, bending, and shear modes must be included. Furthermore, shear deformations can occur easily due to characteristically low transverse shear stiffness of such structures at lower thickness-to-length ratios [26,27]. Therefore, it is crucial to accurately determine the strain and stress fields in the laminated composites.

In general, there are two main approaches to model laminated composite structures: equivalent single layer (ESL) theories and layer-wise (LW) theories. In the LW theories, displacement fields in every single layer are determined independently and then imposed compatibility conditions at the interfaces between laminae to decrease the unknown variables [27–29]. This approach can be used to predict the kinematics and transverse stress fields of the laminated structures accurately. However, in this approach, variables are directly related to the number of layers. This issue can be considered as the method’s main drawback. Therefore, for laminated composites with many layers, the computation cost will be considerably high.

On the other hand, the ESL approach assumes a statically equivalent single layer for a heterogeneous laminated composite and reduces the number of unknowns. Hence, it has significant advantages in simplicity and computational time. In other words, ESL theories are more practical when the primary goal of the analysis is to determine the global behavior of the laminated structures like dynamic responses (fundamental natural frequency, critical buckling load, etc.) [28,30,31].

In both modeling approaches, the governing equations can be derived based on various deformation mechanics and transverse shear stresses as described in the

below sections.

1.2.1 Classical laminated plate deformation theory (CLPT)

The most straightforward plate deformation theory is the classical laminated plate theory (CLPT) [32–35]. This approach is an extended form of Kirchhoff-Love plate theory, and it follows the Kirchhoff theory’s assumptions:

- thickness of the plate does not change after deformation
- straight lines that are normal to the middle surface remain straight after deformation
- straight line perpendicular to the middle surface remain perpendicular

From the first and second assumptions, it is clear that transverse normal displacement is independent of thickness coordinate, and it is neglected ($\epsilon_{zz} = 0$). Furthermore, based on the last assumption, transverse shear strains are considered as zero ($\epsilon_{xz} = 0$, $\epsilon_{yz} = 0$). Therefore, CLPT formulation for analyzing the laminated plate’s kinematics may not be adequate, especially for moderately thick or thick composite structures [28]. Fig 1.5 indicates the cross-section view of a plate’s deformations based on CLPT.

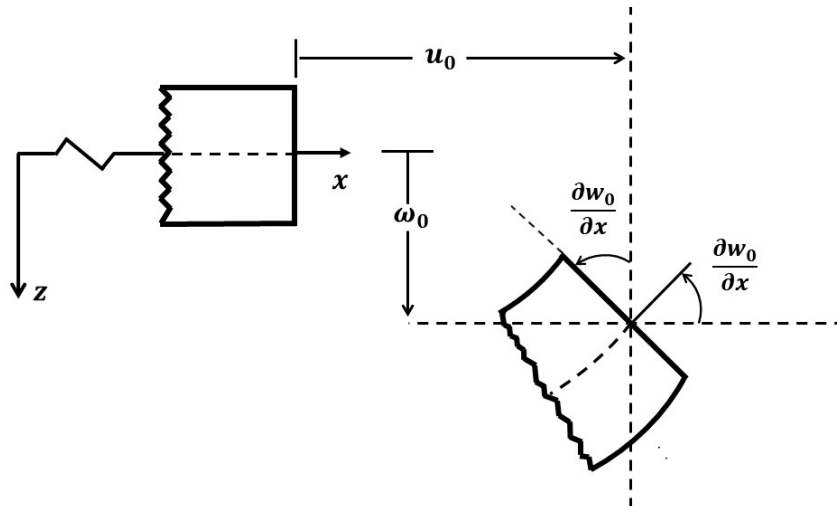


Figure 1.5 Cross-section of undeformed and deformed geometries of a plate based on CLPT

According to the CLPT, deformation of any arbitrary point on the shell in terms of

displacement can be described as:

$$u(x, y, z, t) = u_o(x, y, t) - z \frac{\partial w_o}{\partial x} \quad (1.1)$$

$$v(x, y, z, t) = v_o(x, y, t) - z \frac{\partial w_o}{\partial y} \quad (1.2)$$

$$w(x, y, z, t) = w_o(x, y, t) \quad (1.3)$$

where u , v , and w are the displacements along x , y , and z directions, respectively. In addition subscript ‘o’ denotes the displacement of the middle-surface and z is the distance of an arbitrary point from the neutral surface of the shell, and t is the time variable.

1.2.2 First-order shear deformation theory (FSDT)

The Mindlin-Reissner theory of plate, also known as first-order shear deformation theory (FSDT), is an extension of the Kirchhoff-Love plate theory. The main improvement in this approach is that shear deformations through the thickness of the plate are taken into account in an average sense [28].

In FSDT, straight lines to the reference surface remains straight and inextensible. However, it is no longer remains perpendicular after deformation. Therefore, transverse shear strains are considered as constant through the thickness. Fig 1.6 indicates the deformation of the plate according to the FSDT. [36–43].

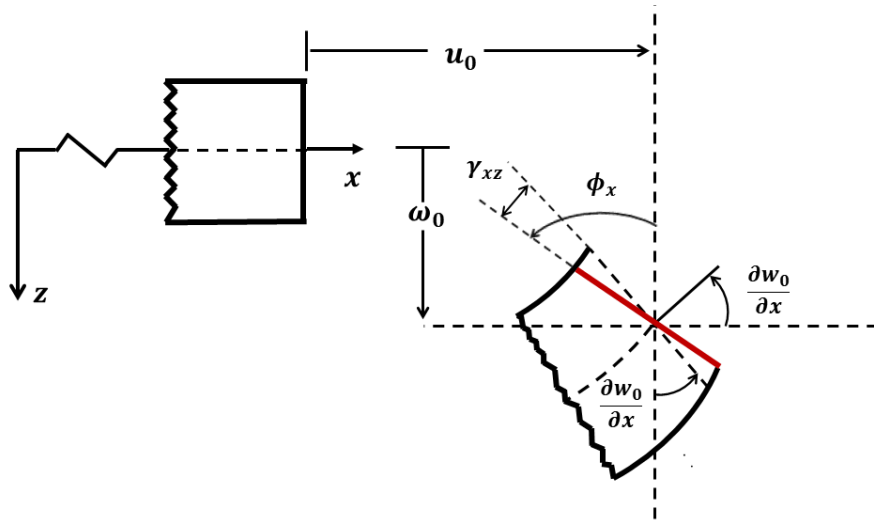


Figure 1.6 Cross-section of undeformed and deformed geometries of a plate based on FSDT

In addition, the kinematic equations for deformation depends on five unknowns, three for middle surface displacement and two for rotations around the x - and y -axis. Since, shear deformation is considered in an average sense, determining a shear correction factor for transverse shear strains is necessary. According to FSDT, deformation of an arbitrary point of the shell can be described in terms of displacements and rotations of the neutral surface as:

$$u(x, y, z, t) = u_o(x, y, t) + z\phi_x(x, y, t) \quad (1.4)$$

$$v(x, y, z, t) = v_o(x, y, t) + z\phi_y(x, y, t) \quad (1.5)$$

$$w(x, y, z, t) = w_o(x, y, t) \quad (1.6)$$

Here, u_o , v_o , and w_o are the displacement of neutral-surface along x , y , and z direction, respectively. In addition, ϕ_x and ϕ_y are normal rotations about the y - z and x - z planes, respectively.

1.2.3 Higher-order shear deformation theory (HSDT)

The higher-order shear deformation theory (HSDT) is developed based on the same hypothesis in CLPT and FSDT. However, one of the main assumption stating that straight lines that are normal to the neutral-surface after deformation have been relaxed [44–51]. Therefore, transverse normal strains are no longer perpendicular and straight to the reference surface after expanding the displacements (u, v, w) as third or higher order functions of the thickness coordinate [27, 28, 30]. Fig 1.7 shows the shear deformation of the plate based on HSDT and the comparison of all mentioned plate theories.

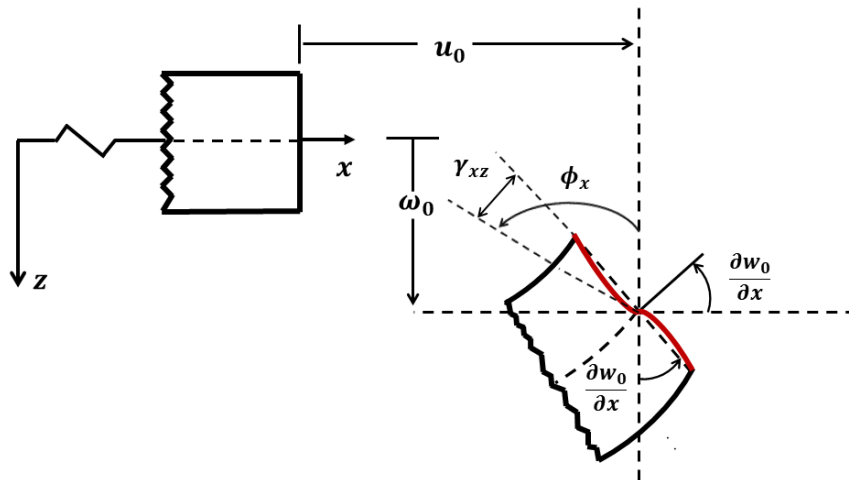


Figure 1.7 Cross-section of undeformed and deformed geometries of a plate based on HSDT

Accordingly, kinematics of plate are described by at least nine independent unknowns. However, these variables can be reduced by imposing certain conditions. For that purpose, traction-free boundary conditions on the top and bottom layers of laminated structures have been imposed [30]. Deformation of a plate according to the kinetics of HSDT can be written as

$$u(x, y, z, t) = u_o(x, y, t) + z\phi_x(x, y, t) + z^3\left(\frac{-4}{3h^2}\right)\left(\phi_x + \frac{\partial w_0}{\partial x}\right) \quad (1.7)$$

$$v(x, y, z, t) = v_o(x, y, t) + z\phi_s(x, y, t) + z^3\left(\frac{-4}{3h^2}\right)\left(\phi_y + \frac{\partial w_0}{\partial y}\right) \quad (1.8)$$

$$w(x, y, z, t) = w_o(x, y, t) \quad (1.9)$$

where h is total thickness of the plate. Although HSDT leads to more accurate results compared to CLPT and FSDT, FSDT provides an acceptable accuracy to capture the dynamic behavior of thin and moderately thick laminated composite structures [28].

1.3 Solution Methods

In literature, various numerical methods are employed to solve the derived governing equations for the composite shell. Finite element (FE) based solution methods are one of the most popular techniques to study the dynamics of laminated composite shells [33, 34, 52–60]. In FE, the continuum domain is divided into a finite number of elements, and finite numbers of parameters specify the behavior of each element. Then, the system matrices can be obtained by an assembly of these elements. For instance, Chakravorty *et al.* [52] analyzed the free and forced vibration of laminated doubly-curved composite shells through FEM. Niyogi *et al.* [10] investigated the vibration response of laminated composite folded plate structures using FEM following FSDT approach. Later, Nguyen-Xuan *et al.* [54] studied free vibration and buckling load of composite sandwich structure through isogeometric FEM method with FSDT approach. In recent years, new FE methods have been presented to increase the efficiency in analyzing the dynamic behavior of laminated composite plates. The FE method uses a weak formulation of the boundary value problem (BVP). When converged, it provides accurate predictions for natural frequencies, mode shapes, and buckling loads; however, a large number of degrees-of-freedom (DOFs) is needed to obtain a precise solution, which imposes a significant computational burden, especially for time-domain response simulations and harmonic solutions. Furthermore,

an arduous effort is required to obtain a suitable mesh [29,61].

To overcome the aforementioned drawbacks of the FE methods, meshless approaches have been proposed. The interpolation in this technique is entirely based on scattered nodes. This unique feature can remove some of the difficulties in FE, such as mesh distortion and remeshing. Smooth particle hydrodynamics [62,63] is one of the initially proposed meshless methods. It is considered an interpolation method based on kernel approximation. Later, Nayroles *et al.* [64] introduced a meshless method called the diffuse element method (DEM). The estimation approach behind this method was moving least square approximations. Later, Belytschko *et al.* [65,66] proposed the element-free Galerkin method. Furthermore, Krysl and Belytschko [67] applied Galerkin method to analyze thin composite shells.

Due to the meshless nature of the mentioned techniques, series-based computational techniques to solve governing equations become more critical. So far, several methods such as Rayleigh-Ritz method [68–71], dynamic stiffness method [48], wave propagation method [51,72,73] were presented for the dynamic behavior analysis of laminated shells and plates. In most of these studies, the computational techniques were initially developed for isotropic structures, then extended to laminated composite ones. Although these techniques are computationally efficient compared to FE, different basis functions are required to satisfy each different boundary conditions.

Recently, Tornabene *et al.* developed several differential quadrature methods (DQM), including generalized differential quadrature (GDQ) [74], local generalized differential quadrature (LGDQ) [75], and moving least square differential quadrature (MLSDQ) [76] methods to study the dynamic response of various complex shell geometries. Although the GQD method is one of the common computationally efficient approaches used in the literature due to its simplicity and versatility, since the derivative and integral operations in the governing equations are performed numerically, the selected basis/trial functions and the sampling scheme highly affect the convergence of the solution and precision of the results.

Therefore, to overcome the limitations of these solution methods, a new meshless approach based on Chebyshev polynomials is developed to study the dynamics of various complex geometries, including beams [77], panels/shells [35, 36, 78], and three-dimensional structures [79–82]. In this method, Chebyshev polynomials, which presents exponential convergence characteristics, are used as the basis to discretize the BVP in either the weak or strong form. Furthermore, the solution can be formulated to directly incorporate the boundary conditions into the solution using the projection matrix approach. Thus, the need to use a different set of basis functions for each different boundary condition is eliminated [77,81,83].

1.4 Design of Composite Structures

Engineers and researchers that are working on laminated composite structures, not only interested in modeling of such structures but they also seek for the best possible design to leverage the flexibility in the design of composite structures [84]. Design quality can be measured based on strength, dynamic stability, *etc.*, that are specific to the application, while the resources are measured based on cost and weight. Traditionally, engineers try to obtain better designs experimentally. Then, a structural modification that improves the performance and reduces the cost or weight has been applied. However, these tasks are tedious and require a high number of trials [9]. Later, mathematical optimization, which includes objective functions, design variables, and constraints, emerged. This procedure deals with changing design variables in order to maximize or minimize an objective function subject to the constraints [85].

In laminated composite materials, lamination layup, which has a significant role in the mechanical properties of laminated composite shells, is a critical issue. Therefore, through layup optimization, the dynamic behavior of laminated composites can be improved. In many studies, fiber orientations and ply thicknesses are considered as design variables. While objective functions can be different such as maximizing critical buckling load, fundamental natural frequency, structural stiffness, and minimizing cost or weight [85]. However, the high number of design variables and vast design space are the main difficulties in the optimization process. To simplify the design variables, lamination parameters that are the material invariants describing the overall stiffness of the structure are introduced by Tsai and Hahn [86,87]. Lamination parameters are basically functions of fiber orientation and ply thickness of each individual layers. Using lamination parameters as design variables not only provides laminate stiffness in a compact form but also offers a convex design space to make the optimization procedure simpler and smoother [9,87].

In this approach, to set a suitable design domain, several feasible regions are introduced and developed through their trigonometric relations and optimization constraints [88–90]. For instance, Diaconu *et. al.* [91] maximized the natural frequency of symmetrically laminated plates using lamination parameters and FSDT. In this study, the design variables are considered as two in-plane and four out-of-plane lamination parameters. Similarly, Trias *et. al.* [92] used optimized lamination parameters for balanced symmetrical laminated plates and cylinders to achieve the maximum fundamental frequency. Recently, Serhat and Basdogan [93] performed a multi-objective optimization by two in-plane lamination parameters for constant-stiffness

laminated plates. In this study, Pareto-optimal solutions were found that maximizes the first natural frequency and buckling load. Furthermore, Serhat *et. al.* [36] maximized the natural frequency of laminated doubly-curved panels through two in-plane lamination parameters and the two-dimensional (2D) spectral Chebyshev method. Also, several researches have been performed on optimization of sandwich composites based on lamination parameters. For example, Kameyama and Fukunga [94] used lamination parameters to optimum design of composite plate wings. In addition, Balabanov *et. al.* [95] designed a sandwich panel through lamination parameters. In this work, they design a lightest weight sandwich structure under a considered buckling load capacity and optimize the face-sheet design based on lamination parameters. Recently, Silva and Meddaikare [96] presented a lamination parameters scheme which are suitable for sandwich and hybrid panels. Considering these design studies, one of the most challenging parts of lamination parameters is retrieving the associated fiber orientations to obtain the closest lamination configuration for the optimized values. For that purpose, several methods have been suggested and used to recover the ply angles through optimization algorithms [9, 97–99]. For instance, Macquart [100] considered twelve lamination parameters linked with a set of blending constraints to achieve manufacturable designs and developed an open-source stacking sequence optimization toolbox, Opti-BLESS, which is based on genetic algorithm (GA).

1.5 Thesis Objective

In this paper, a general two-dimensional (2D) spectral solution method based on Chebyshev polynomials is presented to study the dynamics of laminated composite (truncated) conical shells using lamination parameters and following FSDT assumptions. Note that based on the configuration type of the ply angles, the required number of lamination parameters may change; for instance eight lamination parameters are necessary for symmetric configuration of ply angles.

The derived governing equations were discretized using Gauss-Lobatto sampling algorithm. To impose any type of boundary condition without changing the basis/trial functions, basis recombination (projection matrices) method was implemented. To demonstrate the accuracy and computational efficiency of the presented solution technique, the first ten natural frequencies of three different case studies including straight panels, single curved, and truncated conical shells under two different boundary conditions were investigated. Furthermore, critical buckling load analysis

of straight panels including laminated and sandwich composite structures under two different boundary condition were performed. The results were compared to those obtained using a commercial FE software. To leverage the computational efficiency of the presented meshless approach, first, layup optimization of laminated conical shell to maximize the dimensionless fundamental frequency was carried out for clamped and simply supported edges. Secondly, a parametric analysis was performed to investigate the effect of geometry of the conical shell on the layup optimization.

1.6 Research Contribution

The main contributions of this research are **(i)** developing a modeling framework to predict the dynamic behaviors of the laminated composite shells and **(ii)** to determine the stacking sequence of laminated conical shells to obtain maximum fundamental frequency. Specific contributions can be described as follows:

- Developing a simulation framework based on 2D spectral Chebyshev method and lamination parameters to capture the free vibrations and critical buckling force of laminated composite structures having various geometries including:
 - straight panels
 - cylindrical Shells
 - truncated conical shells
 - straight sandwich panels
- Optimization of the layup for symmetrically laminated conical shells for maximized the fundamental natural frequency, subjected to the non-linear constraints derived from feasible design domain of the lamination parameters. In this optimization study, to reach the optimum composite layups eight lamination parameters including four in-plane and four out of has been considered as design variables.

1.7 Thesis Outline

In the following chapter, the details about the modeling of laminated composite plates, lamination parameters formulation, and governing equations to capture the structure's dynamic behavior are provided. In addition, to solve the derived governing equation, a developed two-dimensional spectral Chebyshev method is presented. Next, to demonstrate the efficiency of the presented analyzing technique, some validation case studies with various geometries, lamination layup, and aspect ratios under different boundary conditions are carried out in Chapter 3. Then in Chapter 4, layup optimization of the laminated conical shell to maximize the fundamental natural frequency of the structure is provided. Also, to show the effects of the geometry on layup optimization of laminated conical shells are investigated. Subsequently, the conclusions and possible directions for future works are presented in Chapters 5 and 6, respectively.

2. Problem Description

This chapter presents the modeling and analysis of laminated composite plates. A laminated truncated conical shell, as a general case study is considered. The governing equations to capture the dynamic behavior of the laminated composite structures was derived. Note that according to the defined geometric parameters, various structure types such as straight panels, cylindrical shells, and sandwich panels can be modeled using the derived governing equations. Finally, the developed solution technique is explained in detail to numerically solve the boundary value problem.

2.1 Laminated Panels and Shells

In this part of study, the schematic of a conical laminated curved panel is illustrated in Fig. 2.1. A cylindrical coordinate frame (x - s - z) is used in the derivation of the governing equations, where x is the coordinate along meridional direction, s is the circumferential direction, and z refers to the thickness direction of the shell. As shown in Fig. (2.1a), α is the semi-vertex of the cone; R_1 and R_2 denotes the radii at the small and big edges of the panel, respectively; L_x , L_s , and h are the lengths of the shell along x and s axes, and thickness along z -axis, respectively. The curvature of the shell is varying as $R_\theta = x \tan(\alpha) + R_1 / \cos(\alpha)$ along the length of the shell (*i.e.* along the x -direction). To estimate the displacement of the conical shell, FSDT assumptions are followed. According to FSDT, deformation of an arbitrary point of the shell can be described in terms of displacements and rotations of the neutral surface.

$$u(x, s, z, t) = u_o(x, s, t) + z\phi_x(x, s, t) \quad (2.1)$$

$$v(x, s, z, t) = v_o(x, s, t) + z\phi_s(x, s, t) \quad (2.2)$$

$$w(x, s, z, t) = w_o(x, s, t) \quad (2.3)$$

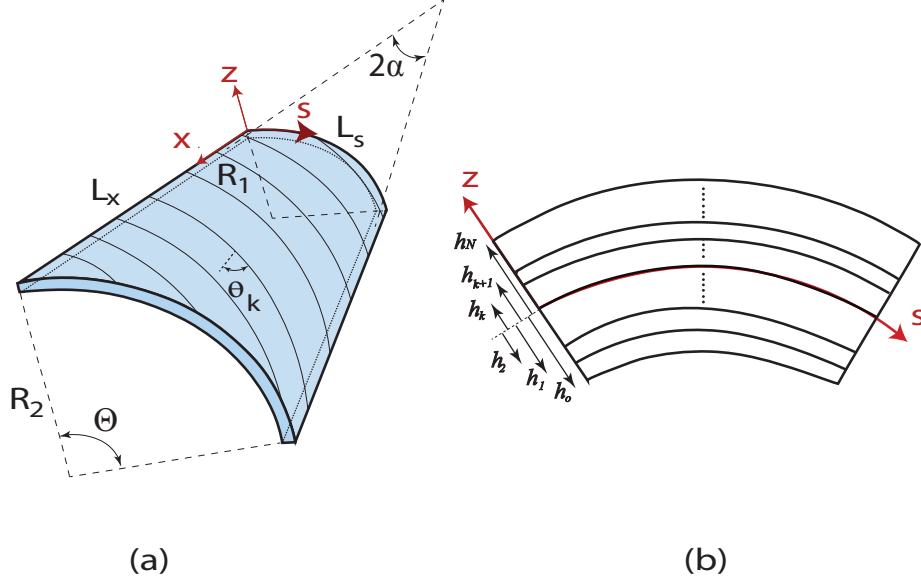


Figure 2.1 Schematics of **(a)** a general curved conical panel geometry and **(b)** cross-section view of the laminated shell.

where u , v , and w are the displacements along x , s , and z directions, respectively. Subscript ‘o’ indicates the deformations of the neutral-surface, ϕ_x and ϕ_s are normal rotations about the s - z and x - z planes, respectively; and z is the distance of an arbitrary point from the neutral surface of the shell, and t is the time variable.

2.1.1 Stiffness formulation using lamination parameters

According to FSDT, the related linear strain equations are given as:

$$\begin{pmatrix} \varepsilon_{xx} \\ \varepsilon_{ss} \\ \gamma_{xs} \\ \gamma_{sz} \\ \gamma_{xz} \end{pmatrix} = \begin{pmatrix} \varepsilon_{xx_o} \\ \varepsilon_{ss_o} \\ \gamma_{xs_o} \\ \gamma_{sz_o} \\ \gamma_{xz_o} \end{pmatrix} + z \begin{pmatrix} k_{xx} \\ k_{ss} \\ k_{xs} \\ 0 \\ 0 \end{pmatrix} \quad (2.4)$$

where ε_{xx_o} , ε_{ss_o} , γ_{xs_o} , γ_{xz_o} , and γ_{sz_o} represent the strains on the neutral surface; and k_{xx} , k_{ss} , k_{xs} are the curvature deformations. The strains and curvature deformations

are related to the deformations of shell as

$$\begin{pmatrix} \varepsilon_{xxo} \\ \varepsilon_{sso} \\ \gamma_{xso} \\ k_{xx} \\ k_{ss} \\ k_{xs} \\ \gamma_{szo} \\ \gamma_{xzo} \end{pmatrix} = \underbrace{\begin{bmatrix} \frac{\partial}{\partial x} & 0 & 0 & 0 & 0 \\ \frac{1}{\mathcal{A}} \frac{\partial \mathcal{A}}{\partial x} & \frac{1}{\mathcal{A}} \frac{\partial}{\partial \theta} & \frac{1}{R_\theta} & 0 & 0 \\ \frac{1}{\mathcal{A}} \frac{\partial}{\partial \theta} & \frac{\partial}{\partial x} - \frac{1}{\mathcal{A}} \frac{\partial \mathcal{A}}{\partial x} & 0 & 0 & 0 \\ 0 & 0 & 0 & \frac{\partial}{\partial x} & 0 \\ 0 & 0 & 0 & \frac{1}{\mathcal{A}} \frac{\partial \mathcal{A}}{\partial x} & \frac{1}{\mathcal{A}} \frac{\partial}{\partial \theta} \\ 0 & 0 & 0 & \frac{1}{\mathcal{A}} \frac{\partial}{\partial \theta} & \frac{\partial}{\partial x} - \frac{1}{\mathcal{A}} \frac{\partial v}{\partial x} \\ 0 & -\frac{1}{R_\theta} & \frac{1}{\mathcal{A}} \frac{\partial}{\partial \theta} & 0 & 1 \\ 0 & 0 & \frac{\partial}{\partial x} & 1 & 0 \end{bmatrix}}_{\mathbf{B}} \begin{pmatrix} u_0 \\ v_0 \\ w_0 \\ \phi_x \\ \phi_s \end{pmatrix} \quad (2.5)$$

where \mathbf{B} is the differential operator matrix and $\mathbf{q} = \{u_0; v_0; w_0; \phi_x; \phi_s\}$ is the displacement vector. \mathcal{A} is the geometry parameter that is determined by the shape of the shell:

- for straight shells, $\mathcal{A} = 1$ and $R_\theta = \infty$
- for cylindrical shells, $\mathcal{A} = R$ and $R_\theta = R$
- for conical shells, $\mathcal{A} = R_1 + x \sin(\alpha)$, $R_\theta = x \tan(\alpha) + R_1 / \cos(\alpha)$

According to Hook's law and the relation between stress and strain ($\boldsymbol{\sigma} = \mathbf{C}\boldsymbol{\varepsilon}$), the constitutive matrix can be expressed as follows:

$$\mathbf{C} = \begin{bmatrix} A_{11} & A_{12} & A_{16} & 0 & 0 & 0 & 0 & 0 \\ A_{12} & A_{22} & A_{26} & 0 & 0 & 0 & 0 & 0 \\ A_{16} & A_{26} & A_{66} & 0 & 0 & 0 & 0 & 0 \\ 0 & 0 & 0 & D_{11} & D_{12} & D_{16} & 0 & 0 \\ 0 & 0 & 0 & D_{12} & D_{22} & D_{26} & 0 & 0 \\ 0 & 0 & 0 & D_{16} & D_{26} & D_{66} & 0 & 0 \\ 0 & 0 & 0 & 0 & 0 & 0 & A_{44}^* & A_{45}^* \\ 0 & 0 & 0 & 0 & 0 & 0 & A_{45}^* & A_{55}^* \end{bmatrix} \quad (2.6)$$

Here, A_{ij} , D_{ij} , and A_{ij}^* are extensional, bending, and transverse shear stiffness entities of laminated composites. Due to the symmetric configuration of the composite layups, extensional and bending coupling stiffness matrices were omitted. However, it should be noticed that, in a sandwich structure, stiffness matrices are considered

as a summation of face-sheets and core parts, which can be described as

$$A = 2A_f + A_c \quad (2.7)$$

$$D = 2D_f + D_c \quad (2.8)$$

$$A^* = 2A_f^* + A_c^* \quad (2.9)$$

In this study, the stiffness properties of laminated structure are obtained through material invariants and lamination parameters as

$$\mathbf{A} = h(\Psi_0 + V_1^A \Psi_1 + V_2^A \Psi_2 + V_3^A \Psi_3 + V_4^A \Psi_4) \quad (2.10)$$

$$\mathbf{D} = \frac{h^3}{12}(\Psi_0 + V_1^D \Psi_1 + V_2^D \Psi_2 + V_3^D \Psi_3 + V_4^D \Psi_4) \quad (2.11)$$

$$\mathbf{A}^* = k_c h(\psi_0 + V_1^A \psi_1 - V_2^A \psi_2) \quad (2.12)$$

where V_i^A and V_i^D ($i = 1, 2, 3, 4$) are extensional and bending lamination parameters, respectively and can be expressed as

$$V_{\{1,2,3,4\}}^A = \frac{1}{h} \sum_{k=1}^N (h_k - h_{k-1}) \left[\cos 2\theta_k, \sin 2\theta_k, \cos 4\theta_k, \sin 4\theta_k \right] \quad (2.13)$$

$$V_{\{1,2,3,4\}}^D = \frac{4}{h^3} \sum_{k=1}^N (h_k^3 - h_{k-1}^3) \left[\cos 2\theta_k, \sin 2\theta_k, \cos 4\theta_k, \sin 4\theta_k \right] \quad (2.14)$$

Here, h_k , θ_k , and h are the thickness and fiber angle of k^{th} layer, and the total thickness of the shell, respectively. In a nutshell, lamination parameters denotes the overall stiffness of laminated composite structures indirectly, in terms of fiber orientation angles, number of layers, and ply thicknesses. Furthermore, in sandwich type structures neutral-axis for face-sheets and core parts are considered as middle plane of the whole structure which can be seen in Fig 2.2. According to that the lamination parameters for laminated sandwich panel can be expressed differently for core and face-sheets.

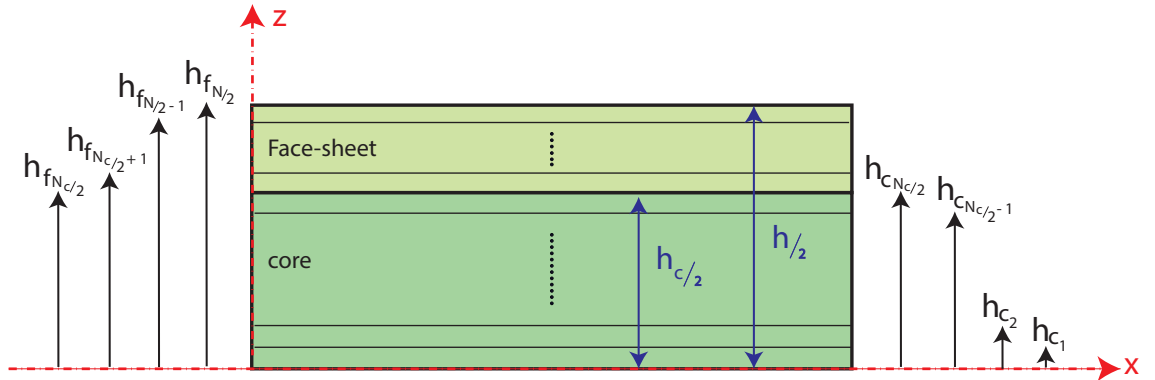


Figure 2.2 cross-section view of the half laminated sandwich shell

$$V_{f_{\{1,2,3,4\}}}^A = \frac{2}{h_f} \sum_{k=N_c/2+1}^{N/2} (h_{f_k} - h_{f_{k-1}}) [\cos 2\theta_{f_k}, \sin 2\theta_{f_k}, \cos 4\theta_{f_k}, \sin 4\theta_{f_k}] \quad (2.15)$$

$$V_{c_{\{1,2,3,4\}}}^A = \frac{2}{h_c} \sum_{k=1}^{N_c/2} (h_{c_k} - h_{c_{k-1}}) [\cos 2\theta_{c_k}, \sin 2\theta_{c_k}, \cos 4\theta_{c_k}, \sin 4\theta_{c_k}] \quad (2.16)$$

$$V_{f_{\{1,2,3,4\}}}^D = \frac{8}{h^3 - h_c^3} \sum_{k=N_c/2+1}^{N/2} (h_{c_k}^3 - h_{c_{k-1}}^3) [\cos 2\theta_{f_k}, \sin 2\theta_{f_k}, \cos 4\theta_{f_k}, \sin 4\theta_{f_k}] \quad (2.17)$$

$$V_{c_{\{1,2,3,4\}}}^D = \frac{8}{h_c^3} \sum_{k=1}^{N_c/2} (h_{c_k}^3 - h_{c_{k-1}}^3) [\cos 2\theta_{c_k}, \sin 2\theta_{c_k}, \cos 4\theta_{c_k}, \sin 4\theta_{c_k}] \quad (2.18)$$

Here, N_c and h_c denote the number of plies and thickness of core part, respectively. Regardless of the exact number of layers, the maximum number of lamination parameters are twelve (twenty four for sandwich) considering FSDT kinematic equations [98, 101]; however, depending on the configuration type of the ply angles, the number of lamination parameters can vary. In the present study, the lamination configuration type of the composite shell is assumed to be symmetric; thus, the stiffness matrix of the shell depends on eight lamination parameters as shown in Eqs. (2.10)-(2.12). The feasible design space is defined by the following nonlinear constraints [90, 99, 102]:

$$2V_1^2(1 - V_3) + 2V_2^2(1 + V_3) + V_3^2 + V_4^2 - 4V_1V_2V_4 \leq 1 \quad (2.19)$$

$$V_1^2 + V_2^2 \leq 1 \quad (2.20)$$

$$-1 \leq V_i \leq 1, \quad (i = 1, \dots, 4) \quad (2.21)$$

In addition, according to Eqs (2.10)-(2.12), Ψ_i ($i = 0, \dots, 4$) and ψ_j ($j = 0, 1, 2$) contains material invariant stiffness parameters, k_c is the shear correction factor. Material invariant components comprise of the material properties (Young's Modulus, shear modulus, and Poisson's ratio) of the structure that are independent of the fiber

angle and can be expressed as

$$\begin{aligned}
\Psi_0 &= \begin{bmatrix} U_1 & U_2 & 0 \\ U_4 & U_1 & 0 \\ 0 & 0 & U_5 \end{bmatrix} & \Psi_1 &= \begin{bmatrix} U_2 & 0 & 0 \\ 0 & -U_2 & 0 \\ 0 & 0 & 0 \end{bmatrix} & \Psi_2 &= \begin{bmatrix} 0 & 0 & \frac{U_2}{2} \\ 0 & 0 & \frac{U_2}{2} \\ \frac{U_2}{2} & \frac{U_2}{2} & 0 \end{bmatrix} \\
\Psi_3 &= \begin{bmatrix} U_3 & -U_3 & 0 \\ -U_3 & U_3 & 0 \\ 0 & 0 & -U_3 \end{bmatrix} & \Psi_4 &= \begin{bmatrix} 0 & 0 & U_3 \\ 0 & 0 & -U_3 \\ U_3 & -U_3 & 0 \end{bmatrix} & & (2.22) \\
\psi_0 &= \begin{bmatrix} U_{11} & 0 \\ 0 & U_{11} \end{bmatrix} & \psi_1 &= \begin{bmatrix} U_{22} & 0 \\ 0 & -U_{22} \end{bmatrix} & \psi_2 &= \begin{bmatrix} 0 & U_{22} \\ U_{22} & 0 \end{bmatrix}
\end{aligned}$$

where

$$\begin{aligned}
U_1 &= \frac{1}{8}(3Q_{11} + 3Q_{22} + 2Q_{12} + 4Q_{66}) & U_{11} &= \frac{1}{2}(Q_{44} + Q_{55}) \\
U_2 &= \frac{1}{2}(Q_{11} - Q_{22}) & U_{22} &= \frac{1}{2}(Q_{44} - Q_{55}) \\
U_3 &= \frac{1}{8}(Q_{11} + Q_{22} - 2Q_{12} - 4Q_{66}) & & (2.23) \\
U_4 &= \frac{1}{8}(Q_{11} + Q_{22} + 6Q_{12} - 4Q_{66}) \\
U_5 &= \frac{1}{8}(Q_{11} + Q_{22} + -2Q_{12} + 4Q_{66})
\end{aligned}$$

Here, Q_{ij} are the lamina stiffness constants that are defined as

$$\begin{aligned}
Q_{11} &= \frac{E_{11}}{(1 - \nu_{12}\nu_{21})} \quad , \quad Q_{22} = \frac{E_{22}}{(1 - \nu_{12}\nu_{21})} \quad , \quad Q_{12} = \frac{\nu_{12}E_{22}}{(1 - \nu_{12}\nu_{21})} & (2.24) \\
Q_{66} &= G_{12} \quad , \quad Q_{44} = G_{23} \quad , \quad Q_{55} = G_{13}
\end{aligned}$$

where E_{11} and E_{22} are the elastic modulus along and perpendicular the fiber direction, respectively. In addition, G_{12} , G_{23} , and G_{31} are shear modulus in $x - y$, $y - z$ and $x - z$ planes, respectively. Furthermore, ν_{12} refer to the major Poisson's ratio of a uni-directional layer.

2.1.2 Derivation of the boundary value problem

The boundary value problem that governs the dynamics of the composite shell can be derived using an energy based approach. The strain energy (E_s) of the laminated shell can be expressed as;

$$E_s = \frac{1}{2} \int_{\mathbb{V}} \boldsymbol{\sigma}^T \boldsymbol{\epsilon} d\mathbb{V} = \frac{1}{2} \int_{\mathbb{A}} \mathbf{q}^T \mathbf{B}^T \mathbf{C} \mathbf{B} \mathbf{q} \mathcal{A} ds dx \quad (2.25)$$

where \mathbb{V} and \mathbb{A} are volume and area of the shell, respectively. Furthermore, panel's kinetic energy (E_k) can be calculated;

$$E_k = \frac{1}{2} \int_{\mathbb{A}} \rho \dot{\mathbf{q}}^T \begin{bmatrix} h & 0 & 0 & 0 & 0 \\ 0 & h & 0 & 0 & 0 \\ 0 & 0 & h & 0 & 0 \\ 0 & 0 & 0 & h^3/12 & 0 \\ 0 & 0 & 0 & 0 & h^3/12 \end{bmatrix} \dot{\mathbf{q}} \mathcal{A} ds dx = \frac{1}{2} \int_{\mathbb{A}} \rho \dot{\mathbf{q}}^T \boldsymbol{\Upsilon} \dot{\mathbf{q}} \mathcal{A} ds dx \quad (2.26)$$

where ρ is the density. Moreover, It must be noticed that, the required kinetic energy for sandwich structures are divided into two parts and written as follows

$$E_k = E_{k_c} + E_{k_f} \quad (2.27)$$

Here, (E_{k_f}) and (E_{k_c}) refer to the face-sheets and core parts kinetic energies, respectively and can be expressed as follow:

$$E_{k_c} = \frac{1}{2} \int_{\mathbb{A}} \rho_c \dot{\mathbf{q}}^T \begin{bmatrix} h_c & 0 & 0 & 0 & 0 \\ 0 & h_c & 0 & 0 & 0 \\ 0 & 0 & h_c & 0 & 0 \\ 0 & 0 & 0 & h_c^3/12 & 0 \\ 0 & 0 & 0 & 0 & h_c^3/12 \end{bmatrix} \dot{\mathbf{q}} dy dx = \frac{1}{2} \int_{\mathbb{A}} \rho_c \dot{\mathbf{q}}^T \boldsymbol{\Upsilon}_c \dot{\mathbf{q}} dy dx \quad (2.28)$$

$$E_{k_f} = \frac{1}{2} \int_{\mathbb{A}} \rho_f \dot{\mathbf{q}}^T \begin{bmatrix} h_f & 0 & 0 & 0 & 0 \\ 0 & h_f & 0 & 0 & 0 \\ 0 & 0 & h_f & 0 & 0 \\ 0 & 0 & 0 & \frac{h^3 - h_c^3}{12} & 0 \\ 0 & 0 & 0 & 0 & \frac{h^3 - h_c^3}{12} \end{bmatrix} \dot{\mathbf{q}} dy dx = \frac{1}{2} \int_{\mathbb{A}} \rho_f \dot{\mathbf{q}}^T \boldsymbol{\Upsilon}_f \dot{\mathbf{q}} dy dx \quad (2.29)$$

Furthermore, the work done by non-conservative forces can be written as:

$$W_{nc} = \frac{1}{2} \int_{\mathbb{A}} h \left[N_{xx} \left(\frac{\partial w_o}{\partial x} \right)^2 + N_{ss} \left(\frac{\partial w_o}{\partial s} \right)^2 \right] \mathcal{A} d\mathbb{A} = \frac{1}{2} \int_{\mathbb{A}} h \mathbf{q}^T \mathbf{B}^T \mathbf{N} \mathbf{B} \mathbf{q} d\mathbb{A} \quad (2.30)$$

where N_{xx} , and N_{ss} are the in-plane stresses along x and s directions, respectively. The integral boundary value problem (IBVP) that governs the dynamic behavior of the curved shells, can be derived using Hamilton's principle as

$$\int_t \int_{\mathbb{V}} \delta(E_k - E_u + W_{nc}) d\mathbb{V} = \int_t \int_{\mathbb{A}} \left(\rho \ddot{\mathbf{q}}^T \mathbf{\Upsilon} \delta \mathbf{q} + \mathbf{q}^T \mathbf{B}^T \mathbf{C} \mathbf{B} \delta \mathbf{q} + h \mathbf{q}^T \mathbf{B}^T \mathbf{N} \mathbf{B} \delta \mathbf{q} \right) \mathcal{A} ds dx = 0 \quad (2.31)$$

2.2 Spectral Chebyshev Approach

To solve the IBVP defined in Eq. (2.31), two-dimensional spectral Chebyshev method, previously developed in [35, 36, 78, 83], is used. Chebyshev polynomials, are recursive and orthogonal polynomials that can be described as [103, 104]:

$$T_k(x) = \cos(k \cos^{-1}(x)) \quad \text{for } k = 0, 1, 2, \dots \quad (2.32)$$

Here, k is an integer. Due to the exponential convergence behavior of Chebyshev polynomials, they are used as the basis for the spatial discretization. Since, the domain of the problem is two-dimensional, the deformation function can be represented by a double expansion of Chebyshev polynomials as

$$q(x, s) = \sum_{k=1}^{N_x} \sum_{l=1}^{N_s} a_{kl} \mathcal{T}_{k-1}(x) \mathcal{T}_{l-1}(s) \quad (2.33)$$

where, a_{kl} 's are expansion coefficients and \mathcal{T} 's are the Chebyshev polynomials of the first kind [103, 104], N_x and N_s are the number of polynomials used along the x and s directions for the truncated expansion. To numerically calculate the dynamic behavior, the domain is discretized using Gauss-Lobatto sampling approach. Since the sampling of the deformation function will lead to a second rank tensor ($q_{kl} =$

$q(x(k), s(l))$), a tensor to vector mapping is applied as

$$q_c = q_{kl}, \quad c = (k-1)N_s + l \quad (2.34)$$

The discretized deflection terms can be expressed as:

$$\mathbf{u}_0 = [\mathbf{I} \mathbf{0} \mathbf{0} \mathbf{0} \mathbf{0}] \mathbf{q} = \mathbf{l}_{\mathbf{u}_0} \mathbf{q} \quad (2.35)$$

$$\mathbf{v}_0 = [\mathbf{0} \mathbf{I} \mathbf{0} \mathbf{0} \mathbf{0}] \mathbf{q} = \mathbf{l}_{\mathbf{v}_0} \mathbf{q} \quad (2.36)$$

$$\mathbf{w}_0 = [\mathbf{0} \mathbf{0} \mathbf{I} \mathbf{0} \mathbf{0}] \mathbf{q} = \mathbf{l}_{\mathbf{w}_0} \mathbf{q} \quad (2.37)$$

$$\phi_x = [\mathbf{0} \mathbf{0} \mathbf{0} \mathbf{I} \mathbf{0}] \mathbf{q} = \mathbf{l}_{\phi_x} \mathbf{q} \quad (2.38)$$

$$\phi_s = [\mathbf{0} \mathbf{0} \mathbf{0} \mathbf{0} \mathbf{I}] \mathbf{q} = \mathbf{l}_{\phi_s} \mathbf{q} \quad (2.39)$$

where \mathbf{I} and $\mathbf{0}$ are $(N_x N_s \times N_x N_s)$ identity and zero matrices, respectively. Note that the vector mapping defined in Eq. (2.34) is also applied to the expansion coefficients (a_{kl}) . Thus, it is possible to define a relationship between the function values at the sampling points and the expansion coefficients as

$$\mathbf{a} = \mathbf{\Gamma}_F \mathbf{q} \quad (2.40)$$

$$\mathbf{q} = \mathbf{\Gamma}_B \mathbf{a} \quad (2.41)$$

where $\mathbf{\Gamma}_F$ and $\mathbf{\Gamma}_B$ are $(N_x N_s \times N_x N_s)$ extended forward and backward transformation matrices, respectively. The derivation of transformation matrices for a one-dimensional function, $f(x)$, the Chebyshev expansion can be written similar to Eq. (2.33) as

$$f(x) = \sum_{k=1}^N a_k \mathcal{T}_{k-1}(x) \quad (2.42)$$

Considering Gauss-Lobatto sampling points, Eq. (2.42) can be written in matrix form as

$$\underbrace{\begin{Bmatrix} f_1 \\ f_2 \\ \vdots \\ f_N \end{Bmatrix}}_{\mathbf{f}} = \underbrace{\begin{bmatrix} \mathcal{T}_0(x_1) & \mathcal{T}_1(x_1) & \dots & \mathcal{T}_{N-1}(x_1) \\ \mathcal{T}_0(x_2) & \mathcal{T}_1(x_2) & \dots & \mathcal{T}_{N-1}(x_2) \\ \vdots & \vdots & \ddots & \vdots \\ \mathcal{T}_0(x_N) & \mathcal{T}_1(x_N) & \dots & \mathcal{T}_{N-1}(x_N) \end{bmatrix}}_{\mathbf{\Gamma}_B} \underbrace{\begin{Bmatrix} a_1 \\ a_2 \\ \vdots \\ a_N \end{Bmatrix}}_{\mathbf{a}} \quad (2.43)$$

Here, $\mathbf{\Gamma}_B$ is the $(N \times N)$ backward transformation matrix. Since, $\mathbf{\Gamma}_B \mathbf{\Gamma}_F = \mathbf{I}$, the forward transformation can be calculated taking the inverse of the backward transformation matrix.

In the case of two-dimensional problem/domain, the forward and backward transformation matrices for each direction are extended through a mapping procedure defined in Eq. (2.34) as

$$\begin{aligned}\mathbb{T}_{B_{c_1 c_2}} &= \Gamma_{B_{k_1 k_2}}^x \Gamma_{B_{l_1 l_2}}^s & (2.44) \\ c_1 &= (k_1 - 1)N_y + l_1, \quad c_2 = (k_2 - 1)N_y + l_2 \\ k_1 &= 1, \dots, N_x, \quad k_2 = 1, \dots, N_x \\ l_1 &= 1, \dots, N_s, \quad l_2 = 1, \dots, N_s\end{aligned}$$

to obtain the $(N_x N_s \times N_x N_s)$ extended forward (\mathbb{T}_F) and backward (\mathbb{T}_B) transformation matrices.

To determine the mass and stiffness matrices from Eqs. (2.31), the integral and derivative operations need to be performed. Note that derivative and integral operations are computed exactly for any function that can be expressed by the Chebyshev expansion given in Eq. (2.33). To calculate the derivative of a function, first its derivative is also expressed as a double expansion of Chebyshev polynomials. It is possible to write a relation between the expansion coefficients of the original function and its derivative as $\mathbf{b} = \mathbf{D}^{q_i} \mathbf{a}$, where \mathbf{D}^{q_i} is the $(N_x N_s \times N_x N_s)$ differentiation matrix with respect to q_i ($q_i = x$ or s).

Using the recursive nature of the Chebyshev polynomials, the derivatives of Chebyshev polynomials can be formulated for a problem defined on $(-1,1)$ as

$$\mathcal{T}'_0(x) = 0 \tag{2.45}$$

$$\mathcal{T}'_1(x) = \mathcal{T}_0(x) \tag{2.46}$$

$$\mathcal{T}'_2(x) = 4\mathcal{T}_1(x) \tag{2.47}$$

$$\mathcal{T}'_{2n-1}(x) = \sum_{m=1}^{n-1} 2(2k-1)\mathcal{T}_{2m}(x) + (2n-1)\mathcal{T}_0(x) \quad \text{if } n > 1 \tag{2.48}$$

$$\mathcal{T}'_{2n}(x) = \sum_{m=1}^n 4k\mathcal{T}_{2m-1}(x) \quad \text{if } n > 1 \tag{2.49}$$

Using the above equations, the $(N \times N)$ derivative matrix (\mathbf{D}) defined on (l_1, l_2) can be obtained through scaling as $\mathbf{D} = 2/(l_2 - l_1)\mathcal{D}$, where \mathcal{D} is the derivative matrix defined on $(-1,1)$.

Note that the derivative matrix obtained for each direction need to be extended for

a two-dimensional domain similar to Eq. (2.44),

$$\begin{aligned} \mathbb{D}_{c_1 c_2}^x &= D_{k_1 k_2}^x & (2.50) \\ c_1 &= (k_1 - 1) N_s + l, \quad c_2 = (k_2 - 1) N_s + l \\ k_1 &= 1, \dots, N_x, \quad k_2 = 1, \dots, N_x, \quad l = 1, \dots, N_s \end{aligned}$$

$$\begin{aligned} \mathbb{D}_{c_1 c_2}^s &= D_{l_1 l_2}^s & (2.51) \\ c_1 &= (k - 1) N_s + l_1, \quad c_2 = (k - 1) N_s + l_2 \\ l_1 &= 1, \dots, N_s, \quad l_2 = 1, \dots, N_s, \quad k = 1, \dots, N_x \end{aligned}$$

Here, \mathbf{D}^x and \mathbf{D}^s are the $(N_x N_s \times N_x N_s)$ extended derivative matrices with respect to x and s , respectively. Then, using the extended transformation matrices, the derivative of a function using its sampled values can be calculated as

$$\mathbf{q}_{,x} = \mathbf{\Gamma}_B \mathbf{b} = \mathbf{\Gamma}_B \mathbf{D}^x \mathbf{a} = \mathbf{\Gamma}_B \mathbf{D}^x \mathbf{\Gamma}_F \mathbf{q} = \mathbf{Q}_x \mathbf{q} \quad (2.52)$$

$$\mathbf{q}_{,s} = \mathbf{\Gamma}_B \mathbf{b} = \mathbf{\Gamma}_B \mathbf{D}^s \mathbf{a} = \mathbf{\Gamma}_B \mathbf{D}^s \mathbf{\Gamma}_F \mathbf{q} = \mathbf{Q}_s \mathbf{q} \quad (2.53)$$

where \mathbf{Q}_x and \mathbf{Q}_s are the $(N_x N_s \times N_x N_s)$ differential matrices with respect to x and s .

To calculate the integral operation, inner product matrix approach is implemented. According to this approach, the multiplication of two functions can be calculated as follows:

$$\int_{\mathbb{A}} f(x, s) g(x, s) d\mathbb{A} = \mathbf{f}^T \mathbf{V} \mathbf{g} \quad (2.54)$$

where \mathbf{V} is the inner product matrix [77]. However, in the case of conical shells, the geometry spatially varies along the length of the shell which necessitates calculation of new inner product matrices to retain the symmetry of the system matrices as

$$\int_{\mathbb{A}} r(x, s) f(x, s) g(x, s) d\mathbb{A} = \mathbf{f}^T \mathbf{V}^r \mathbf{g} \quad (2.55)$$

Here, \mathbf{V}^r is the weighted inner product matrix. Each function in the integral operation has an order of $N_x N_s$ degrees. Therefore, the multiplication of three functions can be expressed as $3N_x 3N_s$. In that case, to obtain the inner product matrix, each function evaluated at $3N_x 3N_s$ sampling point using

$$\mathbf{f}_{3N_x 3N_s} = \mathbf{S}^{x3} \mathbf{S}^{s3} \mathbf{f}_{N_x N_s} \quad (2.56)$$

Here, $\mathbf{S}^{q_{in}}$ is the extrapolation matrix that can be obtained through the derivation

in [77, 80–82]. By putting the Eq. 2.56 in Eq. 2.55 the weighted inner product tensor can be rewritten as

$$\mathbf{v}_{abcde}^r = \sum_{i,j}^{3N_x, 3N_s} \mathbf{v}_i^{3N_x} \mathbf{v}_j^{3N_s} [(\mathbf{S}_{ia}^{x_3} \mathbf{S}_{jb}^{s_3})(\mathbf{S}_{ic}^{x_3} \mathbf{S}_{jd}^{s_3})(\mathbf{S}_{ie}^{x_3} \mathbf{S}_{jf}^{s_3}) r_{gh}] \quad (2.57)$$

Furthermore, To obtain the \mathbf{v}_{abcde}^r tensor, tensor multiplication are employed [105]. To transform \mathbf{v}_{abcde}^r from tensor into a matrix form, mapping algorithm described in Eqs. 2.50 and 2.51 are used.

After discretizing the IBVP and performing derivative and integral operations, the general equation of motion for an unconstrained shell can be obtained as:

$$\mathbf{M}\ddot{\mathbf{q}} + (\mathbf{K} + \mathbf{K}_G)\mathbf{q} = \mathbf{0} \quad (2.58)$$

where \mathbf{M} , \mathbf{K} , and \mathbf{K}_G are mass, elastic stiffness, and geometric stiffness matrices of the structure, respectively. Thus, following the spectral Chebyshev approach, the mass matrix can be obtained as:

$$\mathbf{M} = \begin{bmatrix} \rho h \mathbf{v}^A & \mathbf{0} & \mathbf{0} & \mathbf{0} & \mathbf{0} \\ \mathbf{0} & \rho h \mathbf{v}^A & \mathbf{0} & \mathbf{0} & \mathbf{0} \\ \mathbf{0} & \mathbf{0} & \rho h \mathbf{v}^A & \mathbf{0} & \mathbf{0} \\ \mathbf{0} & \mathbf{0} & \mathbf{0} & \rho \frac{h^3}{12} \mathbf{v}^A & \mathbf{0} \\ \mathbf{0} & \mathbf{0} & \mathbf{0} & \mathbf{0} & \rho \frac{h^3}{12} \mathbf{v}^A \end{bmatrix} \quad (2.59)$$

As it mentioned before, for a sandwich structures mass matrix are accumulation of face-sheets and core's mass matrices and can be described as :

$$\mathbf{M} = \mathbf{M}_f + \mathbf{M}_c \quad (2.60)$$

$$\mathbf{M}_f = \rho_f \begin{bmatrix} h_f \mathbf{v}^A & \mathbf{0} & \mathbf{0} & \mathbf{0} & \mathbf{0} \\ \mathbf{0} & h_f \mathbf{v}^A & \mathbf{0} & \mathbf{0} & \mathbf{0} \\ \mathbf{0} & \mathbf{0} & h_f \mathbf{v}^A & \mathbf{0} & \mathbf{0} \\ \mathbf{0} & \mathbf{0} & \mathbf{0} & \frac{h^3 - h_c^3}{12} \mathbf{v}^A & \mathbf{0} \\ \mathbf{0} & \mathbf{0} & \mathbf{0} & \mathbf{0} & \frac{h^3 - h_c^3}{12} \mathbf{v}^A \end{bmatrix} \quad (2.61)$$

$$\mathbf{M}_c = \rho_c \begin{bmatrix} h_c \boldsymbol{\nu}^A & \mathbf{0} & \mathbf{0} & \mathbf{0} & \mathbf{0} \\ \mathbf{0} & h_c \boldsymbol{\nu}^A & \mathbf{0} & \mathbf{0} & \mathbf{0} \\ \mathbf{0} & \mathbf{0} & h_f \boldsymbol{\nu}^A & \mathbf{0} & \mathbf{0} \\ \mathbf{0} & \mathbf{0} & \mathbf{0} & \frac{h_c^3}{12} \boldsymbol{\nu}^A & \mathbf{0} \\ \mathbf{0} & \mathbf{0} & \mathbf{0} & \mathbf{0} & \frac{h_c^3}{12} \boldsymbol{\nu}^A \end{bmatrix} \quad (2.62)$$

In addition, stiffness matrices of structure can be derived through presented method as:

$$\mathbf{K} = \begin{bmatrix} \mathbf{K}_{11} & \mathbf{K}_{12} & \mathbf{K}_{13} & \mathbf{0} & \mathbf{0} \\ \mathbf{K}_{21} & \mathbf{K}_{22} & \mathbf{K}_{23} & \mathbf{K}_{24} & \mathbf{K}_{25} \\ \mathbf{K}_{31} & \mathbf{K}_{32} & \mathbf{K}_{33} & \mathbf{K}_{34} & \mathbf{K}_{35} \\ \mathbf{0} & \mathbf{K}_{42} & \mathbf{K}_{43} & \mathbf{K}_{44} & \mathbf{K}_{45} \\ \mathbf{0} & \mathbf{K}_{52} & \mathbf{K}_{53} & \mathbf{K}_{54} & \mathbf{K}_{55} \end{bmatrix} \quad (2.63)$$

$$\mathbf{K}_G = \begin{bmatrix} \mathbf{0} & \mathbf{0} & \mathbf{0} & \mathbf{0} & \mathbf{0} \\ \mathbf{0} & \mathbf{0} & \mathbf{0} & \mathbf{0} & \mathbf{0} \\ \mathbf{0} & \mathbf{0} & \mathbf{K}_{G_{33}} & \mathbf{0} & \mathbf{0} \\ \mathbf{0} & \mathbf{0} & \mathbf{0} & \mathbf{0} & \mathbf{0} \\ \mathbf{0} & \mathbf{0} & \mathbf{0} & \mathbf{0} & \mathbf{0} \end{bmatrix} \quad (2.64)$$

where the elements of the elastic and geometric stiffness can be derived as given

below:

$$\begin{aligned}
\mathbf{K}_{11} = & A_{11} \mathbf{Q}_x^T \boldsymbol{\nu}^A \mathbf{Q}_x + A_{12} \sin(\alpha) \boldsymbol{\nu} \mathbf{Q}_x + A_{16} \mathbf{Q}_s^T \boldsymbol{\nu} \mathbf{Q}_x + A_{12} \sin(\alpha) \mathbf{Q}_x^T \boldsymbol{\nu} \\
& + A_{22} \sin^2(\alpha) \boldsymbol{\nu}^{1/A} + A_{26} \sin(\alpha) \mathbf{Q}_s^T \boldsymbol{\nu}^{1/A} + A_{16} \mathbf{Q}_x^T \boldsymbol{\nu} \mathbf{Q}_s + A_{26} \sin(\alpha) \boldsymbol{\nu}^{1/A} \mathbf{Q}_s \\
& + A_{66} \mathbf{Q}_s^T \boldsymbol{\nu}^{1/A} \mathbf{Q}_s
\end{aligned} \tag{2.65}$$

$$\begin{aligned}
\mathbf{K}_{12} = & A_{12} \mathbf{Q}_x^T \boldsymbol{\nu} \mathbf{Q}_s + A_{22} \sin(\alpha) \boldsymbol{\nu}^{1/A} \mathbf{Q}_s + A_{26} \mathbf{Q}_s^T \boldsymbol{\nu}^{1/A} \mathbf{Q}_s + A_{16} \mathbf{Q}_x^T \boldsymbol{\nu} \mathbf{Q}_x \\
& - A_{16} \sin(\alpha) \mathbf{Q}_x^T \boldsymbol{\nu} + A_{26} \sin(\alpha) \boldsymbol{\nu} \mathbf{Q}_x - A_{26} \sin^2(\alpha) \boldsymbol{\nu}^{1/A} + A_{66} \mathbf{Q}_s^T \boldsymbol{\nu} \mathbf{Q}_x \\
& - A_{66} \sin(\alpha) \mathbf{Q}_s^T \boldsymbol{\nu}^{1/A}
\end{aligned} \tag{2.66}$$

$$\mathbf{K}_{13} = A_{12} \mathbf{Q}_x^T \boldsymbol{\nu}^{A/R_\theta} + A_{22} \sin(\alpha) \boldsymbol{\nu}^{1/R_\theta} + A_{26} \mathbf{Q}_s^T \boldsymbol{\nu}^{1/R_\theta} \tag{2.67}$$

$$\begin{aligned}
\mathbf{K}_{22} = & A_{22} \mathbf{Q}_s^T \boldsymbol{\nu}^{1/A} \mathbf{Q}_s + A_{26} \mathbf{Q}_x^T \boldsymbol{\nu} \mathbf{Q}_s - A_{26} \sin(\alpha) \boldsymbol{\nu}^{1/A} \mathbf{Q}_s + A_{26} \mathbf{Q}_s^T \boldsymbol{\nu} \mathbf{Q}_x \\
& - A_{26} \sin(\alpha) \mathbf{Q}_s^T \boldsymbol{\nu}^{1/A} + A_{66} \mathbf{Q}_x^T \boldsymbol{\nu}^A \mathbf{Q}_x - A_{66} \sin(\alpha) \mathbf{Q}_x^T \boldsymbol{\nu} - A_{66} \sin(\alpha) \boldsymbol{\nu} \mathbf{Q}_x \\
& + A_{66} \sin^2(\alpha) \boldsymbol{\nu}^{1/A} + k_c A_{44} \boldsymbol{\nu}^{A/R_\theta^2}
\end{aligned} \tag{2.68}$$

$$\begin{aligned}
\mathbf{K}_{23} = & A_{22} \mathbf{Q}_s^T \boldsymbol{\nu}^{1/R_\theta} + A_{26} \mathbf{Q}_x^T \boldsymbol{\nu}^{A/R_\theta} - A_{26} \sin(\alpha) \boldsymbol{\nu}^{1/R_\theta} - k_c A_{45} \boldsymbol{\nu}^{A/R_\theta} \mathbf{Q}_x \\
& + k_c A_{55} \boldsymbol{\nu}^{1/R_\theta} \mathbf{Q}_s
\end{aligned} \tag{2.69}$$

$$\mathbf{K}_{24} = -k_c A_{45} \boldsymbol{\nu}^{A/R_\theta} \tag{2.70}$$

$$\mathbf{K}_{25} = -k_c A_{55} \boldsymbol{\nu}^{A/R_\theta} \tag{2.71}$$

$$\begin{aligned}
\mathbf{K}_{33} = & A_{22} \boldsymbol{\nu}^{A/R_\theta^2} + k_c A_{44} \mathbf{Q}_x^T \boldsymbol{\nu}^A \mathbf{Q}_x + k_c A_{45} \mathbf{Q}_s^T \boldsymbol{\nu} \mathbf{Q}_x + k_c A_{45} \mathbf{Q}_x^T \boldsymbol{\nu} \mathbf{Q}_s \\
& + k_c A_{55} \mathbf{Q}_s^T \boldsymbol{\nu}^{1/A} \mathbf{Q}_s
\end{aligned} \tag{2.72}$$

$$\mathbf{K}_{34} = k_c A_{44} \mathbf{Q}_x^T \boldsymbol{\nu}^A + k_c A_{45} \mathbf{Q}_s^T \boldsymbol{\nu} \tag{2.73}$$

$$\mathbf{K}_{35} = k_c A_{45} \mathbf{Q}_x^T \boldsymbol{\nu}^A + k_c A_{55} \mathbf{Q}_s^T \boldsymbol{\nu} \tag{2.74}$$

$$\begin{aligned}
\mathbf{K}_{44} = & D_{11} \mathbf{Q}_x^T \boldsymbol{\nu}^A \mathbf{Q}_x + D_{12} \sin(\alpha) \boldsymbol{\nu} \mathbf{Q}_x + D_{16} \mathbf{Q}_s^T \boldsymbol{\nu} \mathbf{Q}_x + D_{12} \sin(\alpha) \mathbf{Q}_x^T \boldsymbol{\nu} \\
& + D_{22} \sin^2(\alpha) \boldsymbol{\nu}^{1/A} + D_{26} \sin(\alpha) \mathbf{Q}_s^T \boldsymbol{\nu}^{1/A} + D_{16} \mathbf{Q}_x^T \boldsymbol{\nu} \mathbf{Q}_s + D_{26} \sin(\alpha) \boldsymbol{\nu}^{1/A} \mathbf{Q}_s \\
& + D_{66} \mathbf{Q}_s^T \boldsymbol{\nu}^{1/A} \mathbf{Q}_s + k_c A_{44} \boldsymbol{\nu}^A
\end{aligned} \tag{2.75}$$

$$\begin{aligned}
\mathbf{K}_{45} = & D_{12} \mathbf{Q}_x^T \boldsymbol{\nu} \mathbf{Q}_s + D_{22} \sin(\alpha) \boldsymbol{\nu}^{1/A} \mathbf{Q}_s + D_{26} \mathbf{Q}_s^T \boldsymbol{\nu}^{1/A} \mathbf{Q}_s + D_{16} \mathbf{Q}_x^T \boldsymbol{\nu}^A \mathbf{Q}_x \\
& - D_{16} \sin(\alpha) \mathbf{Q}_x^T \boldsymbol{\nu} + D_{26} \sin(\alpha) \boldsymbol{\nu} \mathbf{Q}_x - D_{26} \sin^2(\alpha) \boldsymbol{\nu}^{1/A} + D_{66} \mathbf{Q}_s^T \boldsymbol{\nu} \mathbf{Q}_x \\
& - D_{66} \sin(\alpha) \mathbf{Q}_s^T \boldsymbol{\nu}^{1/A} + k_c A_{45} \boldsymbol{\nu}^A
\end{aligned} \tag{2.76}$$

$$\begin{aligned}
\mathbf{K}_{55} = & D_{22} \mathbf{Q}_s^T \boldsymbol{\nu}^{1/A} \mathbf{Q}_s + D_{26} \mathbf{Q}_x^T \boldsymbol{\nu} \mathbf{Q}_s - D_{26} \sin(\alpha) \boldsymbol{\nu}^{1/A} \mathbf{Q}_s + D_{26} \mathbf{Q}_s^T \boldsymbol{\nu} \mathbf{Q}_x \\
& - D_{26} \sin(\alpha) \mathbf{Q}_s^T \boldsymbol{\nu}^{1/A} + D_{66} \mathbf{Q}_x^T \boldsymbol{\nu}^A \mathbf{Q}_x - D_{66} \sin(\alpha) \boldsymbol{\nu} \mathbf{Q}_x + D_{66} \sin^2(\alpha) \boldsymbol{\nu}^{1/A} \\
& + k_c A_{55} \boldsymbol{\nu}^A
\end{aligned} \tag{2.77}$$

$$\mathbf{K}_{\mathbf{G}_{33}} = h (\mathbf{Q}_x^T N_{xx} \boldsymbol{\nu} \mathbf{Q}_x + \mathbf{Q}_s^T N_{ss} \boldsymbol{\nu} \mathbf{Q}_s) \tag{2.78}$$

Note that only the upper triangle part of the stiffness matrices is provided since it is symmetric.

To impose the effect of essential boundary conditions, projection matrices approach is used [77]. In this approach, first, the boundary equations are in matrix form as $\beta \mathbf{q} = \mathbf{0}$. The projection matrix, \mathbf{P} , can be calculated using the singular value decomposition of the β matrix. In a nutshell, the projection matrix defines a coordinate transformation, as

$$\mathbf{q} = \mathbf{P} \mathbf{q}_d \quad (2.79)$$

Thus, inserting Eq. (2.79) into Eq. (2.58), and premultiplying each term with \mathbf{P}^T , the global system matrices can be obtained as

$$\mathbf{M} = \mathbf{P}^T \mathbf{M} \mathbf{P} \quad (2.80)$$

$$\mathbf{K} = \mathbf{P}^T \mathbf{K} \mathbf{P} \quad (2.81)$$

$$\mathbf{K}_G = \mathbf{P}^T \mathbf{K}_G \mathbf{P} \quad (2.82)$$

Subsequently, the natural frequencies (ω), first critical buckling load (λ) and mode shapes (\mathbf{u}) of the system can be calculated using the following eigenvalue problems:

$$\left[\mathbf{K} - \omega^2 \mathbf{M} \right] \mathbf{u} e^{i\omega t} = \mathbf{0} \quad (2.83)$$

$$\left[\mathbf{K} - \lambda \mathbf{K}_G \right] \mathbf{u} = \mathbf{0} \quad (2.84)$$

3. Model Validation and Results

To validate and demonstrate the performance of the presented modeling approach, two main case studies including laminated composite and sandwich structures were investigated. In each case study, the composite structure having various fiber orientations and layup was studied. The analysis in this section has been performed to obtain the first ten natural frequencies and critical buckling load. The (non-dimensionalized) results were compared to those found through the FE method. The relation between the non-dimensional natural frequency ($\bar{\omega}_n$) and the natural frequency (ω_n) of the shell is given by the following formulation:

$$\bar{\omega}_n = \omega_n \left(\frac{L_x^2}{h} \right) \sqrt{\left(\frac{\rho}{E_{22}} \right)} \quad (3.1)$$

Also, dimensionless critical buckling (λ_{cr}) load can be expressed as

$$\lambda_{cr} = \lambda \left(\frac{L_x^2}{h^3 E_{22}} \right) \quad (3.2)$$

It is important to note that, for sandwich structures, E_{22} term used in non-dimensional relations belongs to face-sheet material. The material properties used in the analyses are listed in Table 3.2 for laminated composites, and Tables ?? and ?? for sandwich structures. Note that, the material properties used for laminated composites are non-dimensional [106]. However, for sandwich structures dimensional material properties were utilized [107].

Table 3.1 Material properties of the unidirectional lamina.

E_{11}/E_{22}	15
G_{12}/E_{22} or G_{13}/E_{22}	0.6
G_{23}/E_{22}	0.5
ν	0.25

Table 3.2 Material properties of the unidirectional laminae.

	Graphite/epoxy face-sheets	Glass/epoxy core
E_{11}	181 GPa	38.6 GPa
E_{22}	10.3 GPa	8.27 GPa
G_{12}	7.17 GPa	4.14 GPa
ρ	1600 kg/m ³	1800 kg/m ³
ν_{12}	0.28	0.26

3.1 Laminated Composite Structures

In this part, three case studies including straight panels, curved shells, and truncated conical shells investigated. In each case, free vibration behavior under two different boundary conditions were examined. Besides, for straight panels buckling study performed as well.

3.1.1 Case study I: Straight panel

The geometry of the straight panel is described by the non-dimensional parameters L_s/L_x (aspect ratio) and h/L_x . For a straight panel s direction was corresponded to the y direction. Since, the considered geometry is a straight panel, the geometry parameter \mathcal{A} and the curvature of the panel are set to $\mathcal{A} = 1$ and $R_\theta = \infty$, respectively. Figure 3.1 illustrates the schematics of a 6-layered general laminated straight panel. As seen, s direction in straight panels corresponded to y direction. Here, straight laminated composite panel having different laminate configurations and aspect ratios ($L_y/L_x = 1, 1.5, \text{ and } 2$) were investigated under simply supported ($SSSS$) and fully clamped ($CCCC$) boundary conditions. In each case, the thickness ratio was set to $h/L_x = 0.05$.

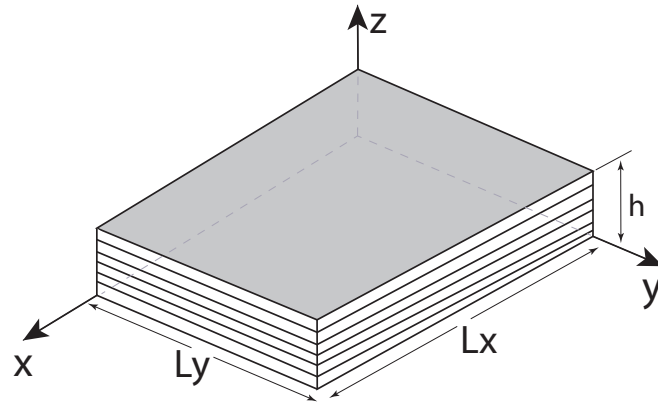


Figure 3.1 Schematics of a laminated straight panel

3.1.1.1 Modal Analysis

In this first case study, the free vibrations of a straight panel/shell was investigated. Prior to validation, a convergence analysis was carried out to determine the required (i) polynomial numbers that need to be used along x and s directions for the presented solution approach, and (ii) element number for FE solution. In this preliminary convergence analysis, a straight laminated composite panel having a geometry of $L_y/L_x = 1$ and $h/L_x = 0.05$, and a layup of $[45/0]_s$ was investigated under $SSSS$ boundary condition. Figure 3.2 shows the stacking sequences of considered case study. The first ten non-dimensional natural frequencies were computed by increasing the polynomial numbers along x and y directions, and listed in Table 3.3. Note that since the investigated panel is a square panel, the polynomial numbers in each axis were kept equal to each other.

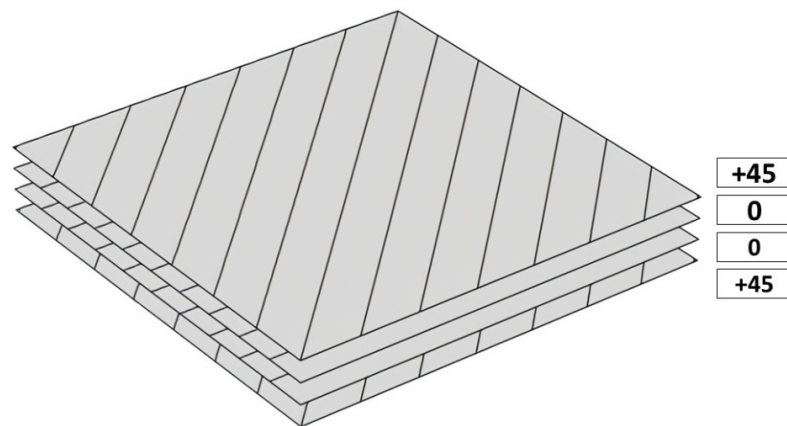


Figure 3.2 Stacking sequence of laminated composite with $[45/0]_s$ layup

As seen from Table 3.3, the presented solution approach is stable and a good con-

Table 3.3 Convergence of the first ten (non-dimensional) natural frequencies for a straight laminated composite panel having a geometry of $L_y/L_x = 1$ and $h/L_x = 0.05$, and a layup of $[45/0]_s$ under $SSSS$ boundary condition.

		Modes									
Method		$\bar{\omega}_1$	$\bar{\omega}_2$	$\bar{\omega}_3$	$\bar{\omega}_4$	$\bar{\omega}_5$	$\bar{\omega}_6$	$\bar{\omega}_7$	$\bar{\omega}_8$	$\bar{\omega}_9$	$\bar{\omega}_{10}$
Present	$N_x = N_s = 6$	12.88	24.96	35.06	42.13	67.40	70.47	75.95	97.27	110.70	117.49
	$N_x = N_s = 7$	12.83	24.80	34.59	39.40	54.94	58.17	64.06	80.90	85.42	112.02
	$N_x = N_s = 8$	12.80	24.77	34.40	39.06	53.77	56.16	63.46	75.45	77.34	88.17
	$N_x = N_s = 9$	12.77	24.76	34.36	38.99	53.27	55.65	63.03	73.49	75.21	86.79
	$N_x = N_s = 10$	12.76	24.76	34.33	38.98	53.21	55.56	62.98	72.85	74.56	85.65
	$N_x = N_s = 11$	12.75	24.76	34.32	38.97	53.19	55.54	62.95	72.73	74.44	85.55
	$N_x = N_s = 12$	12.74	24.76	34.30	38.97	53.19	55.54	62.93	72.70	74.41	85.50
FEM	15×15 elements (5766 DOFs)	12.74	24.76	34.30	38.98	53.21	55.56	62.94	72.75	74.46	85.56

vergence can be obtained even when small polynomial orders are used. To quantitatively assess the level of convergence of the presented solution method for laminated conical composite panels, a thorough investigation was also performed. In this analysis, using the presented solution approach the polynomial numbers along each axis is increased incrementally and the predicted natural frequencies are compared to a reference case (where N_x and N_s are set to 25) using. In order to quantitatively assess the level of convergence the following equation based on logarithmic convergence (LC) has been used

$$LC_{N_x N_s} = \log \left(\frac{1}{n_{\text{modes}}} \sum_{i=1}^{n_{\text{modes}}} \frac{|\bar{\omega}_{N_x N_s}^i - \bar{\omega}_r^i|}{\bar{\omega}_r^i} \right) \quad (3.3)$$

Here, $\bar{\omega}_{N_x N_s}^i$ represents the i^{th} natural frequency calculated with the selected polynomial numbers along x and s -directions (N_x and N_s), $\bar{\omega}_r^i$ represents the i^{th} natural frequency of the reference solution, and n_{modes} shows the number of interested modes. Thus, the convergence of any arbitrary natural frequency or a set of natural frequencies can be investigated using Eq. (3.3).

To visualize how the increase in polynomial numbers affect the convergence, contour maps were plotted in Fig 3.3. Figure 3.3 shows an exemplary contour plot of the LC values (that are averaged for the first ten natural frequencies) for the validation of straight panels under $SSSS$ boundary conditions. Note that to create the contour plots, averaging is used since the LC values are only calculated for integer values of polynomial numbers.

It is possible to determine the required polynomial numbers based on the target accuracy/precision. For instance, if the target accuracy is selected to be 0.1 % compared to the reference, the corresponding LC value will be -3; thereby the polynomial set ($N_x - N_s$) can be determined accordingly from the convergence contour plots. For

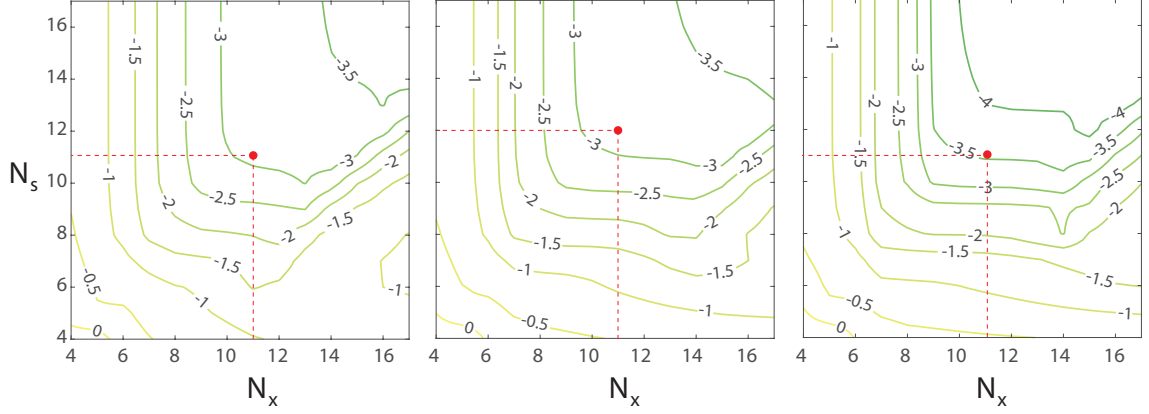


Figure 3.3 Convergence contour plots for the validation of straight panels having $L_y/L_x = 1, 1.5,$ and 2 under $SSSS$ boundary condition

the investigated validation case studies (under $SSSS$ boundary condition), the selected polynomial numbers to satisfy an LC value of -3 can be seen in Figure 3.3. Based on the performed convergence analysis, the polynomial numbers used in the validation simulations are given in Table 3.4.

Table 3.4 Polynomial numbers (N_x-N_s) used in the validation studies based on the convergence analyses.

Case Study	Parameter	Layup	Boundary Condition	
			$SSSS$	$CCCC$
Straight panels	$L_y/L_x = 1$	$[45/0]_s$	11–11	11–11
	$L_y/L_x = 1.5$	$[60/30/0]_s$	11–12	11–12
	$L_y/L_x = 2$	$[90/45/30/0]_s$	11–11	11–11

The polynomial numbers for straight laminated composite panel were selected based on the convergence analyses in Table 3.4. Table 3.5 lists the predicted (non-dimensional) natural frequencies and the corresponding simulation duration obtained using the presented solution technique and the FE results for comparison. The computational duration was measured based on the central processing unit (CPU) time to calculate the first hundred eigenvalues and eigenvectors. Note that a similar convergence study was also performed for the FE simulations. In FE modeling, mapped meshing was used and the modal analysis was performed using MUMPS algorithm. As seen from Table 3.5, there is an excellent agreement between the presented spectral Chebyshev solution and FE method; the maximum and average difference between the predicted results were calculated as 0.22% and 0.03% , respectively. Thus, it can be concluded that the solution approach is as accurate as the FE technique; however since the convergence of the presented method is very rapid, there is a remarkable difference in the computational duration as seen in Table 3.6. Considering all cases, a computational speed-up of around 30 folds was

observed. The main reason for this significant difference in computational duration is the size difference of the obtained system matrices (*i.e.* the significant difference in required DOFs to achieve the same level of accuracy).

Table 3.5 Comparison of the first ten (non-dimensional) natural frequencies of straight composite laminated panels having different aspect ratios and symmetric layup configurations under *SSSS* and *CCCC* boundary conditions.

BC	L_y/L_x	Layup	Method	Modes									
				$\bar{\omega}_1$	$\bar{\omega}_2$	$\bar{\omega}_3$	$\bar{\omega}_4$	$\bar{\omega}_5$	$\bar{\omega}_6$	$\bar{\omega}_7$	$\bar{\omega}_8$	$\bar{\omega}_9$	$\bar{\omega}_{10}$
<i>SSSS</i>	1	[45/0] _s	Present	12.75	24.76	34.32	38.97	53.19	55.54	62.95	72.73	74.44	85.55
			FEM	12.74	24.76	34.30	38.98	53.21	55.56	62.94	72.75	74.46	85.56
	1.5	[60/30/0] _s	Present	8.75	16.27	25.81	26.10	35.69	37.30	49.16	50.10	51.94	59.42
			FEM	8.75	16.27	25.80	26.10	35.68	37.31	49.17	50.11	51.95	59.42
	2	[90/45/30/0] _s	Present	6.71	12.51	21.15	21.86	26.45	32.22	37.77	43.19	44.64	47.93
			FEM	6.71	12.51	21.16	21.86	26.45	32.22	37.74	43.19	44.60	47.98
<i>CCCC</i>	1	[45/0] _s	Present	21.07	34.79	44.92	49.83	64.09	66.77	74.26	83.58	85.68	96.02
			FEM	21.07	34.80	44.93	49.85	64.12	66.80	74.29	83.57	85.68	95.97
	1.5	[60/30/0] _s	Present	15.67	23.73	34.52	35.85	44.95	46.35	58.94	59.16	63.23	69.79
			FEM	15.67	23.73	34.52	35.86	44.96	46.37	58.94	59.16	63.25	69.80
	2	[90/45/30/0] _s	Present	12.87	18.95	28.96	30.60	35.52	40.59	45.70	52.54	55.54	59.09
			FEM	12.87	18.95	28.97	30.63	35.54	40.59	45.67	52.51	55.66	59.22

Table 3.6 Comparison of the required DOFs and the computational cost of validation case studies in Table 3.5.

L_y/L_x	Layup	BC	DOF		Duration (s)	
			Present	FE	Present	FE
1	[45/0] _s	<i>SSSS</i>	605	5766	0.3	8
		<i>CCCC</i>	605	5766	0.3	8
1.5	[60/30/0] _s	<i>SSSS</i>	660	7626	0.4	10
		<i>CCCC</i>	660	7626	0.4	10
2	[90/45/30/0] _s	<i>SSSS</i>	605	5166	0.3	10
		<i>CCCC</i>	605	5166	0.3	10

3.1.1.2 Buckling analysis

In this section, critical compressive buckling forces for laminated straight panels are investigated. As shown Fig 3.4 the buckling analysis performed for uni-axial and bi-axial load types which applied along x -axis (red lines), and x and y -axis (red and blue lines), respectively. The thickness ratio of a 20-layered sandwich structure for all cases has been taken as $h/L_x = 0.05$. Here, straight laminated composite panel having different laminate configurations and aspect ratios ($L_y/L_x = 0.5, 1, 1.5,$ and 2) were studied. Also, the boundary condition for all case studies was considered as all edges simply supported (*SSSS*). The required polynomial numbers for spectral Chebyshev method were selected based on the convergence analysis performed for straight panels in Table 3.4. Therefore, the achieved results from both presented and

the FE methods are listed in Table 3.7. As observed the calculated critical buckling loads using presented approach are in an excellent agreement to the FE results; the maximum and average differences between two methods results are 0.28 % and 0.04 %, respectively. Furthermore, due to the significant reduction in size of system matrices, used number of DOFs and as a result calculation time decreased around 20 folds.

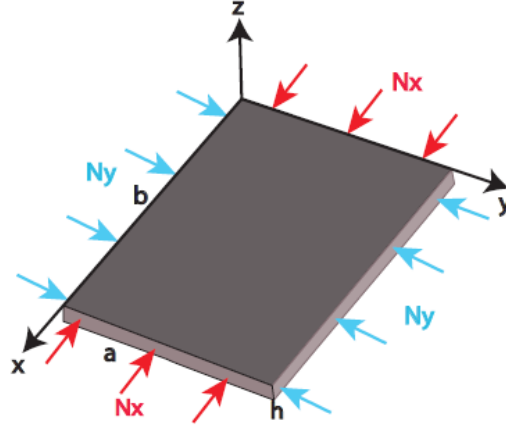


Figure 3.4 Load types in straight laminated composites. Red arrows imply uni-axial loading, and red and blue lines imply bi-axial loading.

3.1.2 Case study II: Cylindrical shell

In this second case study, the free vibration of a cylindrical shell under *SSSS* and *CCCC* boundary conditions were investigated. The aspect and thickness ratios were set to $L_s/L_x = 1$ and $h/L_x = 0.05$, respectively. Since, the considered geometry is a cylindrical shell, the geometry parameter is set to the curvature radius of the panel (*i.e.*, $\mathcal{A} = R = R_1 = R_2$). The analyses were performed for three different curvature amounts ($\Theta = 45^\circ, 60^\circ, \text{ and } 120^\circ$) with various fiber orientations and layup configurations.

The convergence analysis for three curvature amounts under *SSSS* and *CCCC* boundary conditions were performed and the counter plots for *SSSS* boundary conditions were depicted in Fig 3.5. The corresponding polynomial numbers to an average LC value of -3 considering the first ten natural frequencies, obtained and listed in Table 3.8. In that case, the accuracy of selected polynomial sets reach the difference less than 0.1% respect to the reference case. Following the results of convergence studies, required polynomial numbers were determined for each analysis as $N_x-N_s = 11-11$. To validate the results, similar analyses were also performed

Table 3.7 Comparison of the (non-dimensional) critical buckling load of straight composite laminated panels having different aspect ratios and symmetric layup configurations under *SSSS* boundary condition.

Layup	L_y/L_x	Method	λ_{cr}	
			Uni-axial	Bi-axial
[60/30/0] _s	0.5	Present	44.53	19.37
		FEM	44.57	19.38
	1	Present	14.04	7.06
		FEM	14.08	7.07
	1.5	Present	7.26	5.01
		FEM	7.27	5.01
2	Present	5.45	4.34	
	FEM	5.44	4.34	
[90/45/30/0] _s	0.5	Present	49.82	27.91
		FEM	49.83	27.91
	1	Present	16.62	8.37
		FEM	16.62	8.37
	1.5	Present	6.76	4.68
		FEM	6.76	4.68
	2	Present	4.46	4.57
		FEM	4.46	4.57

using FE approach and the required element number was determined as 15×15 . The predicted first ten (non-dimensional) natural frequencies using the presented technique and the FE method are listed in Table 3.9. As seen from Table 3.9, the results are in close agreement; the maximum and average differences between presented method and FE simulation are 0.59 % and 0.13 %, respectively. However, the computational cost of the simulations are significantly reduced (around 27 folds) with the presented spectral approach while preserving the accuracy.

Table 3.8 Polynomial numbers (N_x-N_s) used in the validation studies of cylindrical shells based on the convergence analyses.

Case Study	Parameter	Layup	Boundary Condition	
			<i>SSSS</i>	<i>CCCC</i>
Cylindrical shells	$\Theta = 45^\circ$	[45/0] _s	11-11	11-11
	$\Theta = 60^\circ$	[60/30/0] _s	11-11	11-11
	$\Theta = 120^\circ$	[90/45/30/0] _s	11-11	11-11

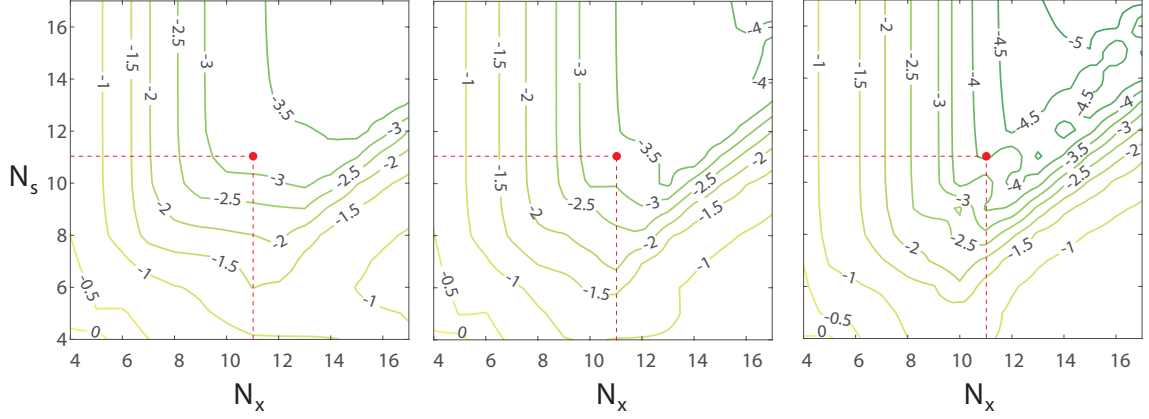


Figure 3.5 Convergence contour plots for the validation of cylindrical shells having $\Theta = 45^\circ, 60^\circ,$ and 120° under *SSSS* boundary condition

Table 3.9 Comparison of the first ten (non-dimensional) natural frequencies of cylindrical composite laminated panels having different curvature amounts and symmetric layup configurations under *SSSS* and *CCCC* boundary conditions.

BC	Θ	Layup	Method	Modes									
				$\bar{\omega}_1$	$\bar{\omega}_2$	$\bar{\omega}_3$	$\bar{\omega}_4$	$\bar{\omega}_5$	$\bar{\omega}_6$	$\bar{\omega}_7$	$\bar{\omega}_8$	$\bar{\omega}_9$	$\bar{\omega}_{10}$
<i>SSSS</i>	45	$[45/0]_s$	Present	26.93	31.33	38.86	44.02	55.35	58.99	65.15	74.53	76.85	86.20
			FEM	26.99	31.36	38.91	44.09	55.39	59.06	65.17	74.57	76.90	86.18
	60	$[60/30/0]_s$	Present	36.46	38.79	45.80	50.76	61.57	64.32	65.95	78.01	80.63	91.17
			FEM	36.46	38.86	45.92	50.88	61.69	64.46	65.97	78.09	80.77	91.26
	120	$[90/45/30/0]_s$	Present	46.90	63.37	73.93	79.19	95.61	96.60	98.32	101.74	106.62	111.28
			FEM	46.84	62.99	73.97	78.92	95.88	96.70	98.78	102.21	106.20	111.78
<i>CCCC</i>	45	$[45/0]_s$	Present	30.71	39.23	48.16	53.51	65.68	69.36	76.29	85.06	87.59	96.41
			FEM	30.71	39.23	48.18	53.52	65.69	69.37	76.32	85.04	87.54	96.32
	60	$[60/30/0]_s$	Present	40.63	45.69	52.04	59.38	71.61	74.32	77.62	88.52	91.31	102.57
			FEM	40.62	45.66	52.05	59.39	71.65	74.35	77.58	88.52	91.34	102.54
	120	$[90/45/30/0]_s$	Present	54.94	68.38	80.34	83.68	101.43	102.44	104.00	109.35	115.71	120.12
			FEM	54.77	68.19	80.17	83.55	101.55	102.43	103.96	109.36	115.46	120.19

3.1.3 Case study III: Conical shell

In the last validation case study of laminated composite panels, free vibrations of a truncated conical composite shell structure under *SSSS* and *CCCC* was investigated. The aspect and thickness ratios, the curvature amount, and the curvature at the short edge were set to $L_s/L_x = \pi/4$, $h/L_x = 0.025$, $\Theta = 2\pi/3$, and $R_1/L_x = 0.375$, respectively. The geometry parameter is set to $\mathcal{A} = R_1 + x \sin(\alpha)$ since the geometry is a conical shell. The analyses were performed for three different vertex angles ($\alpha = 30^\circ, 45^\circ,$ and 60°).

Convergence analysis were carried out for mentioned case studies under *SSSS* and *CCCC* boundary conditions. Figure 3.6 demonstrates the convergence results of truncated conical shells under *SSSS* boundary condition. The polynomial numbers were selected based on the convergence analyses to achieve an average LC value of -3 considering the first ten natural frequencies and listed in Table 3.10. Table 3.11 lists the results of the presented solution approach together with the FE method. As seen, the maximum and average differences between presented method and FE

simulation were calculated as 0.81 % and 0.15 %, respectively. Since the geometry is more complex in this study, the required number of elements to reach the same level of accuracy is higher compared to previous case studies. Thus, the computational speed-ups up to 100 folds can be achieved.

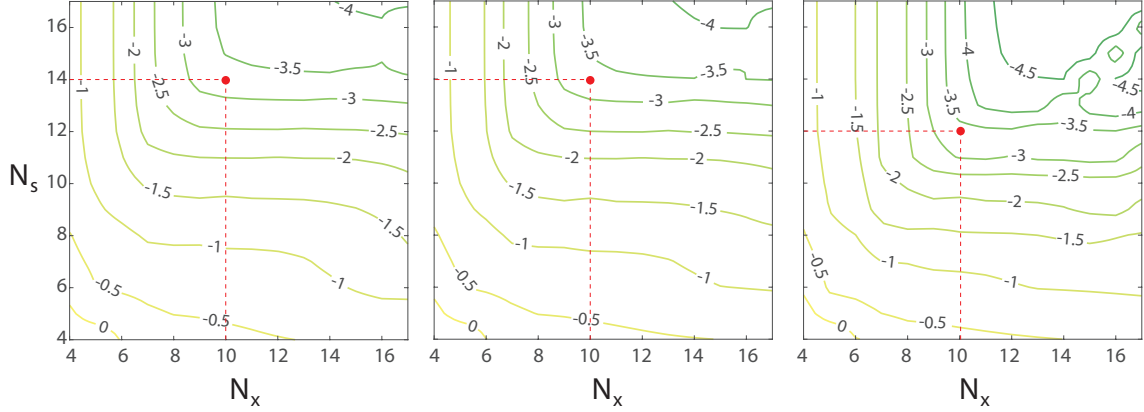


Figure 3.6 Convergence contour plots for the validation of truncated conical panel having $\alpha = 30^\circ$, 45° , and 60° under $SSSS$ boundary condition

Table 3.10 Polynomial numbers (N_x-N_s) used in the validation studies of truncated conical shells based on the convergence analyses.

Case Study	Parameter	Layup	Boundary Condition	
			$SSSS$	$CCCC$
Conical shells	$\alpha = 30^\circ$	$[45/0]_s$	10–14	11–14
	$\alpha = 45^\circ$	$[60/30/0]_s$	10–14	11–14
	$\alpha = 60^\circ$	$[90/45/30/0]_s$	10–12	11–13

Table 3.11 Comparison of the first ten (non-dimensional) natural frequencies of truncated conical composite laminated panels having different apex angles and symmetric layup configurations under $CCCC$ and $SSSS$ boundary conditions.

BC	α	Layup	Method	Modes									
				$\bar{\omega}_1$	$\bar{\omega}_2$	$\bar{\omega}_3$	$\bar{\omega}_4$	$\bar{\omega}_5$	$\bar{\omega}_6$	$\bar{\omega}_7$	$\bar{\omega}_8$	$\bar{\omega}_9$	$\bar{\omega}_{10}$
$SSSS$	30	$[45/0]_s$	Present	49.99	51.99	60.50	70.58	79.13	82.89	85.86	90.55	92.60	99.15
			FEM	50.18	51.98	60.90	70.56	79.23	83.03	86.00	91.00	92.61	99.24
	45	$[60/30/0]_s$	Present	42.95	43.71	52.33	59.87	66.79	69.38	71.88	76.96	79.67	84.90
			FEM	43.15	43.76	52.65	59.90	66.86	69.49	72.04	77.21	79.84	85.03
	60	$[90/45/30/0]_s$	Present	36.06	36.11	46.59	50.09	55.62	57.32	63.44	64.50	75.02	77.90
			FEM	36.11	36.39	46.74	50.16	55.66	57.79	63.36	64.56	75.39	78.08
$CCCC$	30	$[45/0]_s$	Present	56.43	56.66	69.83	76.38	87.62	90.35	93.70	98.77	104.72	111.06
			FEM	56.40	56.61	69.81	76.36	87.59	90.34	93.67	98.72	104.40	110.84
	45	$[60/30/0]_s$	Present	47.90	49.24	60.15	65.29	75.25	77.26	79.10	84.86	91.92	96.77
			FEM	47.88	49.23	60.15	65.28	75.25	77.24	79.08	84.84	91.68	96.62
	60	$[90/45/30/0]_s$	Present	39.75	42.00	52.21	59.74	62.28	63.55	73.36	76.30	86.10	88.46
			FEM	39.75	42.00	52.21	59.74	62.29	63.56	73.37	76.26	86.10	88.44

3.2 Sandwich Structures

The presented spectral Chebyshev method enables to capture the dynamic behavior of laminated sandwich structures as well. Therefore, in this section of study, free vibrations and buckling analysis of straight sandwich panels was performed. Due to the geometric characteristics of the panel, the curvature of the panel and the geometry parameter \mathcal{A} are set to $R_\theta = \infty$ and $\mathcal{A} = 1$, respectively. The geometry of the straight panel is described by the non-dimensional parameters L_y/L_x (aspect ratio), h/L_x and \bar{h}_c/\bar{h}_f . Here, \bar{h}_c and \bar{h}_f denote the thickness of the each layer in sandwich core and face-sheets, respectively. In the this analyses, 20-layered symmetrical straight sandwich panels having different laminate configurations, aspect and thickness ratios under two different boundary conditions *SSSS* and *CCCC* were investigated.

3.2.1 Modal Analysis

In this part, first five (non-dimensional) natural frequency of sandwich structures has been studied. For that purpose the analyses divided into two groups. In the first case study the natural frequencies of sandwich structures with uniform layer thickness ($\bar{h}_c/\bar{h}_f = 1$) are calculated. Then, the identical analyses performed for the sandwich panels with various lamina thicknesses where $\bar{h}_c/\bar{h}_f = 2$. To asses the accuracy of presented method the obtained results compared to those found by the FE method. However, before the natural frequency validation of laminated sandwich panels, a convergence study was carried out. The corresponding LC values for analyses was considered as -3, where the difference between polynomial numbers and reference case must be less than 0.1%. Based on the performed analyses, the polynomial numbers used in the validation study are listed in Table 3.12. Based on the obtained polynomial numbers first five (non-dimensional) natural frequency of laminated sandwich panels are calculated and listed in Table 3.13. As seen from Table 3.13 the result have an agreement with each other. In that case, maximum and average differences between spectral Chebyshev and the FE methods are 0.25% and 0.07%, respectively. Besides, the required DOFs and simulation duration to analyze the free vibrations of the considered model are listed in Table 3.14. As observed, the number of DOFs used to reach the same level of accuracy with the FE method, reduced significantly. Subsequently, the calculation time can speed up around 100 folds.

Table 3.12 Polynomial numbers (N_x-N_s) used in the validation studies of laminated sandwich panels based on the convergence analyses

Thickness ratio	Aspect ratio L_y/L_x	Layup		Boundary condition	
		Face-sheets	Core	<i>SSSS</i>	<i>CCCC</i>
$\bar{h}_c/\bar{h}_f = 1$	1	$[90/\pm 45/0]_s$	$[0_6]_s$	10–9	10–10
	1.5	$[75/60/45/30]_s$	$[\pm 45_6]_s$	10–12	10–12
	2	$[90/-60/30/15]_s$	$[(90/0)6]_s$	9–11	9–13
$\bar{h}_c/\bar{h}_f = 2$	1	$[90/\pm 45/0]_s$	$[0_6]_s$	10–10	10–10
	1.5	$[75/60/45/30]_s$	$[\pm 45_6]_s$	10–11	10–12
	2	$[90/-60/30/15]_s$	$[(90/0)6]_s$	9–10	9–11

Table 3.13 Comparison of the first five (non-dimensional) natural frequencies of straight laminated sandwich panels having different aspect ratios and symmetric layup configurations under *SSSS* and *CCCC* boundary conditions.

BC	\bar{h}_c/\bar{h}_f	L_s/L_x	Layup		Method	Modes				
			Face sheet	core		$\bar{\omega}_1$	$\bar{\omega}_2$	$\bar{\omega}_3$	$\bar{\omega}_4$	$\bar{\omega}_5$
<i>SSSS</i>	1	1	$[90/\pm 45/0]_s$	$[0_6]_s$	Present	13.55	32.33	35.21	53.35	63.39
					FEM	13.55	32.35	35.22	53.37	63.43
		1.5	$[75/60/45/30]_s$	$[\pm 45_6]_s$	Present	8.20	16.60	24.07	27.17	36.91
					FEM	8.21	16.62	24.09	27.20	36.94
		2	$[90/-60/30/15]_s$	$[(90/0)6]_s$	Present	7.74	13.19	22.70	25.79	30.65
					FEM	7.74	13.19	22.70	25.81	30.66
	2	1	$[90/\pm 45/0]_s$	$[0_6]_s$	Present	12.02	29.60	30.07	46.54	58.07
					FEM	12.02	29.62	30.10	46.56	58.08
		1.5	$[75/60/45/30]_s$	$[\pm 45_6]_s$	Present	7.75	15.37	22.48	25.54	32.99
					FEM	7.76	15.39	22.50	25.58	33.03
		2	$[90/-60/30/15]_s$	$[(90/0)6]_s$	Present	7.13	11.72	19.79	23.97	27.93
					FEM	7.13	11.73	19.80	24.00	27.95
<i>CCCC</i>	1	1	$[90/\pm 45/0]_s$	$[0_6]_s$	Present	24.59	47.45	51.52	71.82	83.05
					FEM	24.59	47.47	51.53	71.85	83.07
		1.5	$[75/60/45/30]_s$	$[\pm 45_6]_s$	Present	15.13	25.24	35.18	37.91	48.79
					FEM	15.14	25.26	35.22	37.97	48.85
		2	$[90/-60/30/15]_s$	$[(90/0)6]_s$	Present	15.35	20.98	31.18	38.89	43.68
					FEM	15.35	20.99	31.19	38.93	43.72
	2	1	$[90/\pm 45/0]_s$	$[0_6]_s$	Present	21.63	42.64	43.23	61.39	74.06
					FEM	21.64	42.65	43.27	61.42	74.04
		1.5	$[75/60/45/30]_s$	$[\pm 45_6]_s$	Present	13.98	22.76	32.28	34.59	42.81
					FEM	13.99	22.79	32.33	34.64	42.83
		2	$[90/-60/30/15]_s$	$[(90/0)6]_s$	Present	14.13	18.71	27.13	35.54	39.11
					FEM	14.14	18.73	27.14	35.59	39.01

3.2.2 Buckling analysis

In this part of study, buckling behavior of laminated sandwich panels under *SSSS* boundary condition was investigated. The geometry of the 20-layered sandwich structure can be described by the $L_y/L_x = 1$ and $h/L_x = 0.05$. In addition, according to the Fig 3.4 two different load cases including uni-axial and bi-axial loads applied to the structure. The (non-dimensional) critical buckling loads for different layups and aspect ratios are calculated and obtained result using spectral-Chebyshev method were compared to those found by the FE method. The predicted result using the presented and the FE method are listed in Table 3.15. As it seen,

Table 3.14 Comparison of the required DOFs and the computational cost of validation case studies in Table 3.13.

Layup		L_s/L_x	\bar{h}_c/\bar{h}_f	BC	DOF		Duration (s)	
Face-sheets	Core				Present	FE	Present	FE
[90/±45/0] _s	[0 ₆] _s	1	1	SSSS	450	5766	0.15	15
				CCCC	500	5766	0.15	15
				SSSS	500	5766	0.2	15
				CCCC	500	5766	0.2	15
[75/60/45/30] _s	[±45 ₆] _s	1.5	1	SSSS	600	3906	0.2	10
				CCCC	600	3906	0.2	10
				SSSS	550	3906	0.1	10
				CCCC	600	3906	0.1	10
[90/−60/30/15] _s	[(90/0) ₆] _s	2	1	SSSS	450	5166	0.1	12
				CCCC	465	5166	0.15	12
				SSSS	450	5166	0.1	10
				CCCC	495	5166	0.1	10

the results are quite close together; the maximum and average differences between the presented and the FE methods are 0.14% and 0.08%, respectively. In addition, spectral-Chebyshev technique can reduce the critical buckling load's computational time up to 100 folds.

Table 3.15 Comparison of the (non-dimensional) critical buckling load of straight laminated sandwich panels having different aspect ratios and symmetric layup configurations under *SSSS* boundary condition.

Layup		L_s/L_x	Method	λ_{cr}	
Face-sheets	Core			Uni-axial	Bi-axial
[90/±45/0] _s	[0 ₆] _s	0.5	present	77.81	27.00
			FEM	77.85	27.00
		1	present	20.00	10.00
			FEM	20.01	10.00
		1.5	present	9.94	6.88
			FEM	9.93	6.88
		2	present	7.26	5.81
			FEM	7.26	5.81
[75/60/45/30] _s	[±45 ₆] _s	0.5	present	53.78	25.65
			FEM	53.91	25.71
		1	present	15.29	7.70
			FEM	15.33	7.71
		1.5	present	6.68	4.76
			FEM	6.69	4.77
		2	present	4.81	3.84
			FEM	4.81	3.84

Moreover, to understand the effects of the aspect and thickness ratios on the buckling behavior of the laminated sandwich structure under $SSSS$ boundary condition several case studies were studied and results were plotted in Figs 3.7 and 3.8. The composite layups considered in this section are $[(90/\pm 45/0)_s]_f$ and $[(90/0/90/0)_s]_c$ for face-sheets and core parts, respectively.

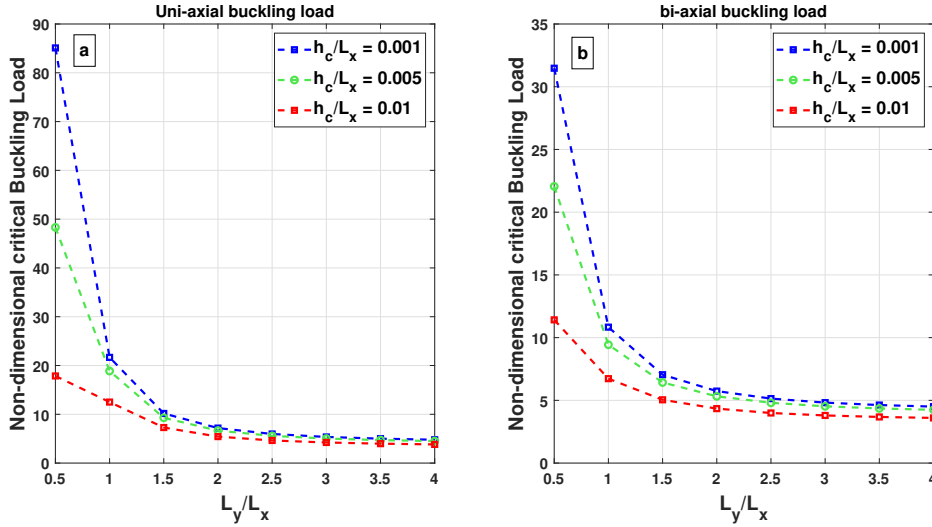


Figure 3.7 Effects of aspect ratios L_y/L_x on non-dimensional critical buckling load under uni-axial (a) and bi-axial (b) buckling forces for uniform layer thickness sandwich

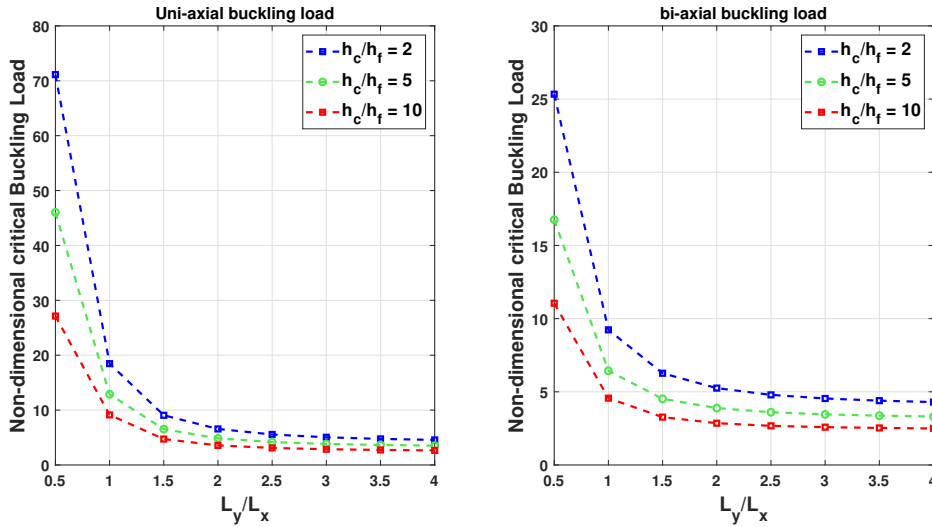


Figure 3.8 Effects of aspect ratios L_y/L_x on non-dimensional critical buckling load under uni-axial (a) and bi-axial (b) buckling forces for variable layer thicknesses sandwich $[(90/\pm 45/0)/(90/0)_2]_s$ layup

In Fig 3.7 the variation in uni-axial and bi-axial buckling load as a function of plate aspect ratio (L_y/L_x) with uniform lamina thickness ($h_c = h_f$) is depicted for three different thickness ratios ($\bar{h}_c/L_x = 0.001, 0.005, 0.01$). As seen from Fig 3.7, by increasing the thickness of each layer, both uni-axial and bi-axial critical buckling

loads has been decreased. In addition, for higher aspect ratios, the effect of thickness on buckling behavior of the structure is insignificant.

In Fig 3.8, the same procedure has been followed. However, the thickness of each lamina is no longer uniform. In that case, different thickness ratios ($h_c/h_f = 2, 5, 10$) has been considered and their effects on variation of uni-axial and bi-axial buckling load were investigated. As it expected, by increasing the thickness and aspect ratios non-dimensional critical buckling load has been reduced for both uni-axial and bi-axial load cases.

4. Design of Laminated Composite Panels

4.1 Fundamental Frequency Maximization

The presented solution approach is a promising technique to be used in the design of composite panels due to its remarkable computational efficiency. In the design of composite panels, the main objective is to determine the optimum lamination parameters that meet the target design requirements. Once the optimum lamination parameters are found, they can be used to determine the ply angles and stacking sequence.

To maximize the fundamental natural frequency, the optimization problem can be formulated as

$$\begin{aligned} \min : \quad & f(X) = -\bar{\omega}_o \\ \text{find : } \quad & X_{opt} = \{V_1^A, V_2^A, V_3^A, V_4^A, V_1^D, V_2^D, V_3^D, V_4^D\} \\ \text{subject to : } \quad & \text{Eqs. (2.19) – (2.21)} \end{aligned} \quad (4.1)$$

Here, lamination parameters that determine the fiber orientation angles are considered as design variables. The nonlinear constraint equations, Eqs. (2.19)-(2.21), define the feasible design space. Note that lamination parameters provide a convex design space for the most physical quantities such as natural frequency or buckling load [87, 93]. To solve the optimization problem, interior point method in *fmincon* solver of MATLAB is used. In the optimization solution, the origin of the feasible design space is set to be the initial guesses. As a numerical example, a (truncated) conical panel having the geometry of $\alpha = 60^\circ$, $L_s/L_x = 2\pi/3$, $h/L_x = (0.05 \text{ and } 0.1)$, and $R_1/L_x = (0.5, 1)$ under *CSCS* boundary condition (edges along x -direction are clamped and s -direction are simply supported) was investigated. Figure 4.1 demonstrates a 8-layered conical panel with $h/L_x = 0.05$ and $R_1/L_x = 0.5$ geometry characteristics.

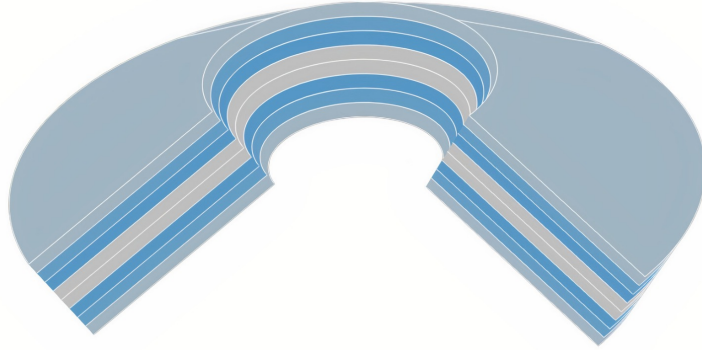


Figure 4.1 8-layered laminated truncated conical shell with $\alpha = 60^\circ$, $L_s/L_x = 2\pi/3$, $h/L_x = 0.05$ and $R_1/L_x = 0.5$ geometry properties

The lamination parameters that maximizes the fundamental frequency were calculated and listed in Table 4.1. Note that the optimization simulation only reveals the lamination parameters; however, the fiber angles and stacking sequence need to be identified afterwards. For that purpose, a symmetric layup with constant layer thicknesses was considered for all the cases and the corresponding ply angles and stacking sequence was found using Opti-BLESS toolbox [100] and listed in Table 4.2 together with the differences compared to the maximum natural frequencies obtained using lamination parameters. In that case, to demonstrate the effects of the retrieved fiber angles on maximum fundamental frequencies, fiber orientations with increments of 15° and 1° were considered. Although, the most common fiber orientation in composite design and production are 0° , $\pm 45^\circ$, and 90° , fibers with 15° resolution are manufacturable as well. As the number of layers are increased, the results obtained with the determined layup get close to the calculated optimum values. However, there exists no clear tendency in the results when fiber orientations with 15° and 1° increments are used.

Table 4.1 Optimized lamination parameters and the corresponding fiber angles and stacking sequence of laminated conical shell under $CSCS$ boundary conditions that maximizes non-dimensional fundamental frequency.

	$h/L_x = 0.05$		$h/L_x = 0.1$	
	$R_1/L_x = 0.5$	$R_1/L_x = 1$	$R_1/L_x = 0.5$	$R_1/L_x = 1$
V_1^A	-0.2277	-0.3026	-0.3024	-0.34391
V_2^A	0.0003	-0.0024	-0.0001	-0.0006
V_3^A	-0.8960	-0.8163	-0.8170	-0.76178
V_4^A	0.0002	0.0018	0.0001	0.00058
V_1^D	0.5955	0.8340	0.7113	0.90597
V_2^D	0.0002	-0.0006	-0.0001	-0.00017
V_3^D	-0.2902	0.3917	0.0122	0.64183
V_4^D	-0.0009	-0.0013	0.0001	-0.00034
$(\lambda_o)_{opt}$	27.29	24.85	18.88	17.64

Table 4.2 Optimal layups considering 15° and 1° angle increments.

	N	Optimal layup (15° angle increments)	Diff. (%)	Optimal layup (1° angle increments)	Diff. (%)
$h/L_x = 0.05$ $R_1/L_x = 0.5$	4	$[45/-45]_s$	11.95	$[36/-39]_s$	14.29
	8	$[30/-30/-45/60]_s$	4.62	$[-25/34/-58/52]_s$	4.36
	12	$[15/-30/-45/45/60/-60]_s$	3.37	$[23/-28/-44/53/-55/51]_s$	3.74
	16	$[15/-30/45/-45/45/-45/60/-60]_s$	3.59	$[-12/31/-46/46/-51/52/53/-53]_s$	3.63
$h/L_x = 0.05$ $R_1/L_x = 1.0$	4	$[0/45]_s$	6.04	$[4/-47]_s$	5.88
	8	$[0/-45/45/45]_s$	8.09	$[5/-41/53/-54]_s$	5.67
	12	$[0/15/-45/-45/60/45]_s$	5.51	$[-8/19/-49/54/53/-52]_s$	5.63
	16	$[0/0/45/-45/45/-45/-60/60]_s$	5.51	$[-1/-4/42/-51/52/-52/53/-52]_s$	5.79
$h/L_x = 0.1$ $R_1/L_x = 0.5$	4	$[15/-45]_s$	7.89	$[-25/39]_s$	12.45
	8	$[-15/45/-60/45]_s$	4.56	$[-11/39/-55/53]_s$	3.71
	12	$[0/45/-45/-45/-60/60]_s$	3.87	$[8/-33/51/-54/-55/55]_s$	3.65
	16	$[-15/15/45/-45/45/60/-60/-45]_s$	4.08	$[8/-21/43/-50/52/-53/-54/54]_s$	3.81
$h/L_x = 0.1$ $R_1/L_x = 1$	4	$[0/-45]_s$	3.97	$[2/-48]_s$	3.74
	8	$[0/45/-60/60]_s$	4.48	$[-6/31/58/-52]_s$	4.31
	12	$[0/0/-45/45/-60/60]_s$	3.12	$[3/-9/47/52/-53/-53]_s$	4.14
	16	$[0/0/-30/45/-60/-60/45/60]_s$	4.02	$[-3/-5/26/57/-52/54/-52/-51]_s$	4.42

4.2 Effect of Geometry on Fundamental Frequency Maximization

To analyze the effect of geometry such as vertex angle and panel curvature on the optimized ply angles and stacking sequence for fundamental frequency of laminated conical shell, we performed a parametric case study leveraging the high computational efficiency of the presented solution approach. In the analyses, the constant geometry values were set to $L_s/L_x = \pi/4$ and $h/L_x = 0.05$. In the first part, the effect of curvature amount (Θ) on maximized fundamental frequency of a conical shell under $SSSS$ and $CCCC$ boundary conditions were studied for several semi-vertex angles ($\alpha = 15^\circ, 30^\circ, 45^\circ$, and 60°) and the results are shown in Fig. 4.2. In the second part, the effect of vertex angle (α) on maximized fundamental frequency of a conical shell under $SSSS$ and $CCCC$ boundary conditions were studied for several curvature amounts ($\Theta = 30^\circ, 45^\circ, 60^\circ, 90^\circ$, and 120°) and the results are shown

in Fig. 4.3. Note that for each individual value of semi-vertex angle and curvature amount, we performed the optimization problem defined by Eq. (4.1). Thus, optimal layups of each point is different. To exemplify, Table 4.3 lists the corresponding optimal layups for the geometries shown by the dashed red curves in Figs. 4.2 and 4.3.

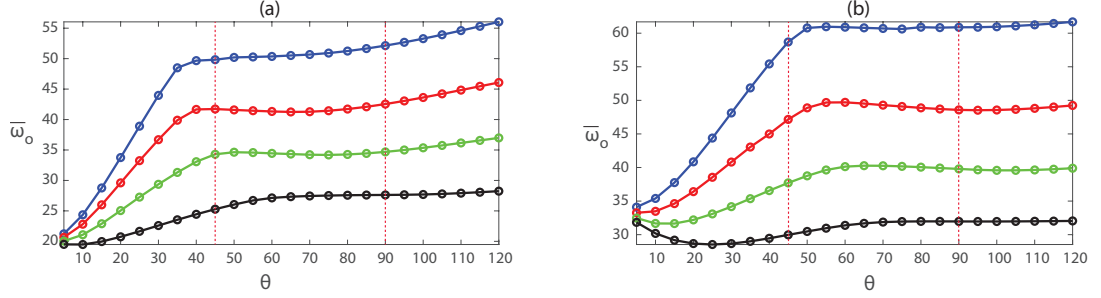


Figure 4.2 Effect of curvature amount (Θ) on maximized natural frequency, $(\bar{\omega}_o)_{\max}$, of a conical panel having $L_s/L_x = \pi/4$ and $h/L_x = 0.05$ under (a) *SSSS* and (b) *CCCC* boundary conditions for various semi-vertex angle. Blue, red, green, and black lines represent the semi-vertex angles of 15° , 30° , 45° , and 60° , respectively.

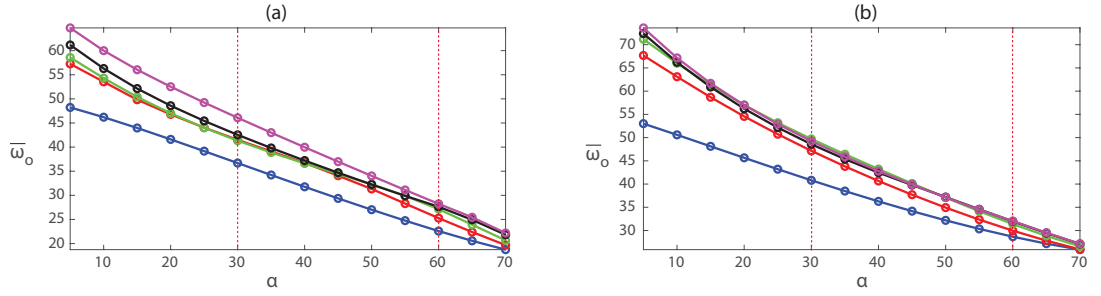


Figure 4.3 Effect of semi-vertex angle (α) on maximized natural frequency, $(\bar{\omega}_o)_{\max}$, of a conical panel having $L_s/L_x = \pi/4$ and $h/L_x = 0.05$ under (a) *SSSS* and (b) *CCCC* boundary conditions. Blue, red, green, black, and magenta lines represent the curvature amount of 30° , 45° , 60° , 90° , and 120° , respectively.

Table 4.3 Optimal layups considering 12 layers and 15° angle increments for the selected geometries shown by the dashed red curves in Figs. 4.2 and 4.3.

Geometry	BC: SSSS		BC: CCCC	
	Optimal layup	Diff. (%)	Optimal layup	Diff. (%)
$\alpha = 15^\circ, \theta = 45^\circ$	[90/90/-60/60/60/-60] _s	0.40 %	[90/90/90/90/90/90] _s	0.55 %
$\alpha = 15^\circ, \theta = 90^\circ$	[90/90/45/-45/-45/45] _s	5.27 %	[90/90/-45/45/45/-45] _s	3.96 %
$\alpha = 30^\circ, \theta = 30^\circ$	[-45/45/90/90/90/90] _s	8.42 %	[90/0/90/90/90/90] _s	3.19 %
$\alpha = 30^\circ, \theta = 45^\circ$	[75/-60/-75/60/-75/75] _s	0.14 %	[90/0/90/90/90/90] _s	2.33 %
$\alpha = 30^\circ, \theta = 60^\circ$	[90/-60/60/45/45/-45] _s	2.15 %	[90/90/-45/45/75/-75] _s	1.23 %
$\alpha = 30^\circ, \theta = 90^\circ$	[75/-60/-45/45/45/-45] _s	1.94 %	[90/90/-45/45/-45/45] _s	2.39 %
$\alpha = 30^\circ, \theta = 120^\circ$	[60/-60/-60/60/-45/45] _s	0.54 %	[90/90/-45/45/45/-45] _s	2.72 %
$\alpha = 45^\circ, \theta = 45^\circ$	[-45/45/90/90/90/90] _s	3.81 %	[0/90/90/90/90/90] _s	1.38 %
$\alpha = 45^\circ, \theta = 90^\circ$	[-60/60/45/-45/60/-60] _s	0.84 %	[90/90/45/-45/-45/45] _s	1.84 %
$\alpha = 60^\circ, \theta = 30^\circ$	[-45/45/90/90/90/90] _s	6.91 %	[90/0/90/90/90/90] _s	1.71 %
$\alpha = 60^\circ, \theta = 45^\circ$	[45/-45/90/90/90/90] _s	5.85 %	[0/0/90/90/90/90] _s	3.37 %
$\alpha = 60^\circ, \theta = 60^\circ$	[-45/45/90/90/90/90] _s	3.76 %	[0/0/90/90/90/90] _s	3.03 %
$\alpha = 60^\circ, \theta = 90^\circ$	[45/-45/-60/60/75/-60] _s	1.63 %	[0/-75/60/-60/60/90] _s	1.25 %
$\alpha = 60^\circ, \theta = 120^\circ$	[45/-45/-60/60/-60/75] _s	1.49 %	[0/-60/60/60/-60/45] _s	3.25 %

As seen from both plots, increasing the semi-vertex angle decreases the maximized fundamental frequency monotonically. On the other hand, the effect of curvature amount is complex. For instance, increasing the curvature amount increases the maximized fundamental frequency if the semi-vertex angle is smaller than 40° . However, as can be seen in Fig. 4.2, increasing the curvature amount higher than 40° does not effect the maximized natural frequencies significantly.

5. Conclusion

This paper presents a spectral modeling approach to accurately predict the dynamics of laminated composite structures. In this solution technique, FSDT kinematic equations were followed and the spatial discretization was performed using Chebyshev polynomials (of the first kind). To describe the stiffness properties of the laminate, eight lamination parameters (in-plane and bending) were used since laminate configuration was assumed to be symmetric. Then, the discretized equations of motion were derived following the Galerkin's method to obtain the system matrices of the composite panel.

To demonstrate the accuracy and performance of the presented technique, several case studies including straight, cylindrical, truncated conical, and sandwich panels were investigated. The predicted (non-dimensional) natural frequencies and critical buckling loads were compared to those obtained using a commercial FE software. Considering all the validation case studies, maximum differences in predicted free vibration and critical buckling load results are 0.8% of 0.3%, respectively. Thus, it can be concluded that the presented solution approach enables predicting the dynamics of laminated composite structures as accurate as an FE approach, yet at a fraction of the computational time. The main reason of these speed-ups is the significant decrease in the required DOFs and the size of the system matrices. In that case, calculation time for natural frequency analyses reduced to around 100 folds. While, in critical buckling load study this computational time can be decreased around 100-150 folds.

To leverage the rapid convergence of the solution approach, we also performed optimization case studies to design laminated conical shells for maximum fundamental frequency. Since the lamination parameter approach leads a convex design space, a gradient base optimization approach was employed to find the optimum lamination parameters. In this optimization procedure, the main goal of optimization was to maximize the fundamental frequency of the laminated conical shell subjected to the non-linear constraint, which was derived from the feasible design space's lamination parameters. In this study, eight lamination parameters were considered as the prob-

lem's design variables (due to the symmetric configuration). Then, the corresponding fiber angles and the stacking sequence were determined using the Opti-BLESS toolbox which is based on the genetic algorithm optimization in MATLAB. Based on the performed analyses, as the number of layers, the predicted natural frequencies for the determined ply angles converges to the maximized natural frequencies obtained using the lamination parameters. For that purpose, symmetrical laminated conical shells with various aspect ratios, thickness ratios, boundary conditions and layer numbers was investigated. However, there is not much differences in the natural frequencies corresponding to the optimal layups for 15° and 1° angle increments. Subsequently, a parametric study to demonstrate the effects of semi-vertex angle and curvature on maximized natural frequency were carried out. From the analyses, it can be concluded that using proper layup optimization plays a crucial role in the dynamic performance improvement of laminated composite shells significantly.

6. Future Work

Modeling and analyzing the dynamics of composite structures is a highly challenging subject. In addition, to achieve a better performance in composite material, structural optimization plays a vital role. In this thesis, to predict the dynamic behavior of the laminated composite shells and sandwich panels, a two-dimensional spectral-Chebyshev technique was developed and combined with lamination parameters. Furthermore, a single objective optimization study has been performed to obtain a maximum natural frequency of a laminated conical shell. However, capturing the dynamics of composites, including complex geometries and layups, demands considerable effort. Thus, the future work of this study can be expressed by improving the versatility and robustness of the presented method. For instance, different plate geometries, such as discontinuous shells which exist in the industry, can be modeled through the improved spectral Chebyshev method. In addition, to achieve a better structural performance, an effective multi-objective optimization using the presented method and lamination parameters is proposed. Reducing structure weight and cost, maximizing the frequency gaps, and maximizing critical buckling loads can be the main goals of this optimization problems. Subsequently, to increase the efficiency of the analysis, the aforementioned numerical study can be extended to experimental research.

Bibliography

- [1] D. D. Chung, Composite materials: science and applications, Springer Science & Business Media, 2010.
- [2] C. T. Herakovich, Mechanics of composites: a historical review, *Mechanics Research Communications* 41 (2012) 1–20.
- [3] L. A. Carlsson, D. F. Adams, R. B. Pipes, Experimental characterization of advanced composite materials, CRC press, 2014.
- [4] S. W. Lee, *Advances in Thick Section Composite and Sandwich Structures*, Springer, 2020.
- [5] F. L. Matthews, R. D. Rawlings, Composite materials: engineering and science, CRC press, 1999.
- [6] L. P. Kollar, G. S. Springer, *Mechanics of composite structures*, Cambridge university press, 2003.
- [7] M. K. Buragohain, *Composite structures: design, mechanics, analysis, manufacturing, and testing*, CRC press, 2017.
- [8] T. W. Clyne, D. Hull, *An introduction to composite materials*, Cambridge university press, 2019.
- [9] Z. Gürdal, R. T. Haftka, P. Hajela, *Design and optimization of laminated composite materials*, John Wiley & Sons, 1999.
- [10] A. Guha Niyogi, M. Laha, P. Sinha, Finite element vibration analysis of laminated composite folded plate structures, *Shock and Vibration* 6 (5, 6) (1999) 273–283.
- [11] I. Kreja, A literature review on computational models for laminated composite and sandwich panels, *Central European Journal of Engineering* 1 (1) (2011) 59–80.
- [12] G. Udupa, S. S. Rao, K. Gangadharan, Functionally graded composite materials: an overview, *Procedia Materials Science* 5 (2014) 1291–1299.
- [13] N. Zhang, T. Khan, H. Guo, S. Shi, W. Zhong, W. Zhang, Functionally graded materials: an overview of stability, buckling, and free vibration analysis, *Advances in Materials Science and Engineering* 2019 (2019).

- [14] S. K. Bohidar, R. Sharma, P. R. Mishra, Functionally graded materials: A critical review, *International Journal of Research* 1 (4) (2014) 289–301.
- [15] J. Vinson, *The behavior of sandwich structures of isotropic and composite materials*, Routledge, 2018.
- [16] A. Johnson, G. Sims, Mechanical properties and design of sandwich materials, *Composites* 17 (4) (1986) 321–328.
- [17] O. T. Thomsen, E. Bozhevolnaya, A. Lyckegaard, *Sandwich Structures 7: Advancing with Sandwich Structures and Materials: Proceedings of the 7th International Conference on Sandwich Structures*, Aalborg University, Aalborg, Denmark, 29-31 August 2005, Springer Science & Business Media, 2005.
- [18] L. A. Carlsson, G. A. Kardomateas, *Structural and failure mechanics of sandwich composites*, Vol. 121, Springer Science & Business Media, 2011.
- [19] V. Birman, G. A. Kardomateas, Review of current trends in research and applications of sandwich structures, *Composites Part B: Engineering* 142 (2018) 221–240.
- [20] M. Abachizadeh, M. Tahani, An ant colony optimization approach to multi-objective optimal design of symmetric hybrid laminates for maximum fundamental frequency and minimum cost, *Structural and Multidisciplinary Optimization* 37 (4) (2009) 367–376.
- [21] M. Savran, L. Aydin, Stochastic optimization of graphite-flax/epoxy hybrid laminated composite for maximum fundamental frequency and minimum cost, *Engineering Structures* 174 (2018) 675–687.
- [22] S. Adali, V. Verijenko, Optimum stacking sequence design of symmetric hybrid laminates undergoing free vibrations, *Composite structures* 54 (2-3) (2001) 131–138.
- [23] H. Hemmatian, A. Fereidoon, H. Shirdel, Optimization of hybrid composite laminate based on the frequency using imperialist competitive algorithm, *Mechanics of Advanced Composite Structures* 1 (1) (2014) 37–48.
- [24] M. Tahani, F. Kolahan, A. Sarhadi, Genetic algorithm for multi-objective optimal design of sandwich composite laminates with minimum cost and maximum frequency, in: *International Conference on Advances in Materials, Product Design & Manufacturing Systems (ICMPM 2005)*, 2005.
- [25] H. Sekine, H. Shirahata, M. Matsuda, Vibration characteristics of composite sandwich plates and layup optimization of their laminated frp composite faces, *Advanced Composite Materials* 14 (2) (2005) 181–197.
- [26] S. Abrate, M. Di Sciuva, *1.16 multilayer models for composite and sandwich structures* (2018).
- [27] J. Reddy, R. Arciniega, Shear deformation plate and shell theories: from stavsky to present, *Mechanics of Advanced Materials and Structures* 11 (6) (2004) 535–582.

- [28] J. N. Reddy, *Mechanics of laminated composite plates and shells: theory and analysis*, CRC press, 2003.
- [29] K. M. Liew, X. Zhao, A. J. Ferreira, A review of meshless methods for laminated and functionally graded plates and shells, *Composite Structures* 93 (8) (2011) 2031–2041.
- [30] J. Reddy, D. Robbins Jr, *Theories and computational models for composite laminates* (1994).
- [31] S. Abrate, M. Di Sciuva, Equivalent single layer theories for composite and sandwich structures: A review, *Composite Structures* 179 (2017) 482–494.
- [32] F. Ebrahimi, A. Rastgo, An analytical study on the free vibration of smart circular thin fgm plate based on classical plate theory, *Thin-Walled Structures* 46 (12) (2008) 1402–1408.
- [33] S. Shojaee, N. Valizadeh, E. Izadpanah, T. Bui, T.-V. Vu, Free vibration and buckling analysis of laminated composite plates using the nurbs-based isogeometric finite element method, *Composite Structures* 94 (5) (2012) 1677–1693.
- [34] S. Sarrami-Foroushani, M. Azhari, Nonlocal vibration and buckling analysis of single and multi-layered graphene sheets using finite strip method including van der waals effects, *Physica E: Low-dimensional Systems and Nanostructures* 57 (2014) 83–95.
- [35] G. Serhat, B. Bediz, I. Basdogan, Unifying lamination parameters with spectral-tchebychev method for variable-stiffness composite plate design, *Composite Structures* 242 (2020) 112183.
- [36] G. Serhat, M. R. Anamagh, B. Bediz, I. Basdogan, Dynamic analysis of doubly curved composite panels using lamination parameters and spectral-tchebychev method, *Computers & Structures* 239 (2020) 106294.
- [37] Ö. Civalek, Vibration analysis of laminated composite conical shells by the method of discrete singular convolution based on the shear deformation theory, *Composites Part B: Engineering* 45 (1) (2013) 1001–1009.
- [38] Y. Kiani, R. Dimitri, F. Tornabene, Free vibration study of composite conical panels reinforced with fg-cnts, *Engineering Structures* 172 (2018) 472–482.
- [39] H. Li, F. Pang, X. Wang, Y. Du, H. Chen, Free vibration analysis for composite laminated doubly-curved shells of revolution by a semi analytical method, *Composite Structures* 201 (2018) 86–111.
- [40] X. Xiang, J. Guoyong, L. Wanyou, L. Zhigang, A numerical solution for vibration analysis of composite laminated conical, cylindrical shell and annular plate structures, *Composite Structures* 111 (2014) 20–30.
- [41] L. Zhang, Z. Lei, K. Liew, Free vibration analysis of functionally graded carbon nanotube-reinforced composite triangular plates using the fsdt and element-free imls-ritz method, *Composite Structures* 120 (2015) 189–199.

- [42] A. Shooshtari, S. Razavi, A closed form solution for linear and nonlinear free vibrations of composite and fiber metal laminated rectangular plates, *Composite Structures* 92 (11) (2010) 2663–2675.
- [43] R. Chiriac, M. Vrabie, The first order shear deformation theory for sandwich plates, *INTERSECTII/INTERSECTIONS* 13 (1) (2016) 37–47.
- [44] S. Boutaleb, K. H. Benrahou, A. Bakora, A. Algarni, A. A. Bousahla, A. Tounsi, A. Tounsi, S. Mahmoud, Dynamic analysis of nanosize fg rectangular plates based on simple nonlocal quasi 3d hsd, *Advances in nano research* 7 (3) (2019) 191.
- [45] M. Medani, A. Benahmed, M. Zidour, H. Heireche, A. Tounsi, A. A. Bousahla, A. Tounsi, S. Mahmoud, Static and dynamic behavior of (fg-cnt) reinforced porous sandwich plate using energy principle, *Steel and Composite Structures* 32 (5) (2019) 595–610.
- [46] H. Sayyaadi, M. A. A. Farsangi, An analytical solution for dynamic behavior of thick doubly curved functionally graded smart panels, *Composite Structures* 107 (2014) 88–102.
- [47] T. Park, S.-Y. Lee, J. Seo, G. Voyiadjis, Structural dynamic behavior of skew sandwich plates with laminated composite faces, *Composites Part B: Engineering* 39 (2) (2008) 316–326.
- [48] F. A. Fazzolari, A refined dynamic stiffness element for free vibration analysis of cross-ply laminated composite cylindrical and spherical shallow shells, *Composites Part B: Engineering* 62 (2014) 143–158.
- [49] E. Viola, F. Tornabene, N. Fantuzzi, General higher-order shear deformation theories for the free vibration analysis of completely doubly-curved laminated shells and panels, *Composite Structures* 95 (2013) 639–666.
- [50] C. H. Thai, L. V. Tran, D. T. Tran, T. Nguyen-Thoi, H. Nguyen-Xuan, Analysis of laminated composite plates using higher-order shear deformation plate theory and node-based smoothed discrete shear gap method, *Applied Mathematical Modelling* 36 (11) (2012) 5657–5677.
- [51] A. Ferreira, C. Roque, P. Martins, Radial basis functions and higher-order shear deformation theories in the analysis of laminated composite beams and plates, *Composite structures* 66 (1-4) (2004) 287–293.
- [52] D. Chakravorty, J. Bandyopadhyay, P. Sinha, Finite element free vibration analysis of doubly curved laminated composite shells, *Journal of Sound and Vibration* 191 (4) (1996) 491–504.
- [53] M. H. Izadi, S. Hosseini-Hashemi, M. H. Korayem, Analytical and fem solutions for free vibration of joined cross-ply laminated thick conical shells using shear deformation theory, *Archive of Applied Mechanics* 88 (12) (2018) 2231–2246.

- [54] H. Nguyen-Xuan, C. H. Thai, T. Nguyen-Thoi, Isogeometric finite element analysis of composite sandwich plates using a higher order shear deformation theory, *Composites Part B: Engineering* 55 (2013) 558–574.
- [55] A. K. Sharma, N. Mittal, Free vibration analysis of laminated composite plates with elastically restrained edges using fem, *Central European journal of engineering* 3 (2) (2013) 306–315.
- [56] C. Thai-Hoang, N. Nguyen-Thanh, H. Nguyen-Xuan, T. Rabczuk, An alternative alpha finite element method with discrete shear gap technique for analysis of laminated composite plates, *Applied Mathematics and Computation* 217 (17) (2011) 7324–7348.
- [57] F.-K. Chang, J. L. Perez, K.-Y. Chang, Analysis of thick laminated composites, *Journal of Composite Materials* 24 (8) (1990) 801–822.
- [58] Y. Cho, R. Averill, First-order zig-zag sublaminated plate theory and finite element model for laminated composite and sandwich panels, *Composite structures* 50 (1) (2000) 1–15.
- [59] A. Masud, M. Panahandeh, Finite-element formulation for analysis of laminated composites, *Journal of engineering mechanics* 125 (10) (1999) 1115–1124.
- [60] S. Serdoun, S. Hamza Cherif, Vibration analysis of composite and sandwich plates reinforced with parabolic fibers using an alternative hierarchical finite element method, *Journal of Sandwich Structures & Materials* 22 (4) (2020) 1074–1110.
- [61] F. Tornabene, N. Fantuzzi, F. Ubertini, E. Viola, Strong formulation finite element method based on differential quadrature: a survey, *Applied Mechanics Reviews* 67 (2) (2015).
- [62] L. B. Lucy, A numerical approach to the testing of the fission hypothesis, *The astronomical journal* 82 (1977) 1013–1024.
- [63] R. A. Gingold, J. J. Monaghan, Smoothed particle hydrodynamics: theory and application to non-spherical stars, *Monthly notices of the royal astronomical society* 181 (3) (1977) 375–389.
- [64] B. Nayroles, G. Touzot, P. Villon, Generalizing the finite element method: diffuse approximation and diffuse elements, *Computational mechanics* 10 (5) (1992) 307–318.
- [65] T. Belytschko, Y. Krongauz, D. Organ, M. Fleming, P. Krysl, Meshless methods: an overview and recent developments, *Computer methods in applied mechanics and engineering* 139 (1-4) (1996) 3–47.
- [66] T. Belytschko, L. Gu, Y. Lu, Fracture and crack growth by element free galerkin methods, *Modelling and Simulation in Materials Science and Engineering* 2 (3A) (1994) 519.

- [67] P. Krysl, T. Belytschko, Analysis of thin plates by the element-free galerkin method, *Computational Mechanics* 17 (1) (1995) 26–35.
- [68] G. Jin, T. Ye, Y. Chen, Z. Su, Y. Yan, An exact solution for the free vibration analysis of laminated composite cylindrical shells with general elastic boundary conditions, *Composite Structures* 106 (2013) 114–127.
- [69] G. Jin, T. Ye, X. Jia, S. Gao, A general fourier solution for the vibration analysis of composite laminated structure elements of revolution with general elastic restraints, *Composite Structures* 109 (2014) 150–168.
- [70] T. Ye, G. Jin, Z. Su, X. Jia, A unified chebyshev–ritz formulation for vibration analysis of composite laminated deep open shells with arbitrary boundary conditions, *Archive of Applied Mechanics* 84 (4) (2014) 441–471.
- [71] X. Song, Q. Han, J. Zhai, Vibration analyses of symmetrically laminated composite cylindrical shells with arbitrary boundaries conditions via rayleigh–ritz method, *Composite Structures* 134 (2015) 820–830.
- [72] A. Ferreira, C. Roque, P. Martins, Analysis of composite plates using higher-order shear deformation theory and a finite point formulation based on the multiquadric radial basis function method, *Composites Part B: Engineering* 34 (7) (2003) 627–636.
- [73] A. Ferreira, A formulation of the multiquadric radial basis function method for the analysis of laminated composite plates, *Composite structures* 59 (3) (2003) 385–392.
- [74] F. Tornabene, A. Liverani, G. Caligiana, Fgm and laminated doubly curved shells and panels of revolution with a free-form meridian: a 2-d gdq solution for free vibrations, *International Journal of Mechanical Sciences* 53 (6) (2011) 446–470.
- [75] F. Tornabene, N. Fantuzzi, M. Baccocchi, The local gdq method applied to general higher-order theories of doubly-curved laminated composite shells and panels: the free vibration analysis, *Composite Structures* 116 (2014) 637–660.
- [76] F. Tornabene, Retracted: Free vibrations of laminated composite doubly-curved shells and panels of revolution via the gdq method (2011).
- [77] B. Yagci, S. Filiz, L. L. Romero, O. B. Ozdoganlar, A spectral-tchebychev technique for solving linear and nonlinear beam equations, *Journal of Sound and Vibration* 321 (1-2) (2009) 375–404.
- [78] M. R. Anamagh, B. Bediz, Free vibration and buckling behavior of functionally graded porous plates reinforced by graphene platelets using spectral chebyshev approach, *Composite Structures* 253 (2020) 112765.
- [79] S. Filiz, B. Bediz, L. Romero, O. B. Ozdoganlar, A spectral-tchebychev solution for three-dimensional vibrations of parallelepipeds under mixed boundary conditions, *Journal of applied mechanics* 79 (5) (2012).

- [80] S. Filiz, B. Bediz, L. Romero, O. B. Ozdoganlar, Three dimensional dynamics of pretwisted beams: A spectral-tchebychev solution, *Journal of Sound and Vibration* 333 (10) (2014) 2823–2839.
- [81] B. Bediz, Three-dimensional vibration behavior of bi-directional functionally graded curved parallelepipeds using spectral tchebychev approach, *Composite Structures* 191 (2018) 100–112.
- [82] M. R. Anamagh, B. Bediz, Three-dimensional dynamics of functionally graded and laminated doubly-curved composite structures having arbitrary geometries and boundary conditions, *Composites Part B: Engineering* 172 (2019) 533–546.
- [83] B. Bediz, A spectral-tchebychev solution technique for determining vibrational behavior of thick plates having arbitrary geometry, *Journal of Sound and Vibration* 432 (2018) 272–289.
- [84] A. L. Kalamkarov, A. G. Kolpakov, *Analysis, design and optimization of composite structures*, Vol. 1, Wiley New York, 1997.
- [85] S. Nikbakt, S. Kamarian, M. Shakeri, A review on optimization of composite structures part i: Laminated composites, *Composite Structures* 195 (2018) 158–185.
- [86] H. T. Hahn, S. W. Tsai, *Introduction to composite materials*, CRC Press, 1980.
- [87] H. Fukunaga, H. Sekine, M. Sato, A. Iino, Buckling design of symmetrically laminated plates using lamination parameters, *Computers & structures* 57 (4) (1995) 643–649.
- [88] M. W. Bloomfield, C. Diaconu, P. Weaver, On feasible regions of lamination parameters for lay-up optimization of laminated composites, *Proceedings of the Royal Society A: Mathematical, Physical and Engineering Sciences* 465 (2104) (2009) 1123–1143.
- [89] M. Miki, Y. Sugiyama, Optimum design of laminated composite plates using lamination parameters, *AIAA journal* 31 (5) (1993) 921–922.
- [90] S. Setoodeh, M. Abdalla, Z. Gurdal, Approximate feasible regions for lamination parameters, in: *11th AIAA/ISSMO multidisciplinary analysis and optimization conference*, 2006, p. 6973.
- [91] C. Diaconu, M. Sato, H. Sekine, Layup optimization of symmetrically laminated thick plates for fundamental frequencies using lamination parameters, *Structural and multidisciplinary Optimization* 24 (4) (2002) 302–311.
- [92] D. Trias, P. Maimi, N. Blanco, Maximization of the fundamental frequency of plates and cylinders, *Composite Structures* 156 (2016) 375–384.
- [93] G. Serhat, I. Basdogan, Multi-objective optimization of composite plates using lamination parameters, *Materials & Design* 180 (2019) 107904.

- [94] M. Kameyama, H. Fukunaga, Optimum design of composite plate wings for aeroelastic characteristics using lamination parameters, *Computers & structures* 85 (3-4) (2007) 213–224.
- [95] V. Balabanov, O. Weckner, M. Epton, G. Mabson, S. Cregger, A. Blom, Optimal design of a composite sandwich structure using lamination parameters, in: 53rd AIAA/ASME/ASCE/AHS/ASC Structures, Structural Dynamics and Materials Conference 20th AIAA/ASME/AHS Adaptive Structures Conference 14th AIAA, 2012, p. 1520.
- [96] G. H. Silva, Y. Meddaikar, Lamination parameters for sandwich and hybrid material composites, *AIAA Journal* 58 (10) (2020) 4604–4611.
- [97] X. Tong, W. Ge, X. Gao, Y. Li, Optimization of combining fiber orientation and topology for constant-stiffness composite laminated plates, *Journal of Optimization Theory and Applications* 181 (2) (2019) 653–670.
- [98] A. Viquerat, A continuation-based method for finding laminated composite stacking sequences, *Composite Structures* 238 (2020) 111872.
- [99] S. Setoodeh, M. M. Abdalla, Z. Gürdal, Design of variable-stiffness laminates using lamination parameters, *Composites Part B: Engineering* 37 (4-5) (2006) 301–309.
- [100] T. Macquart, Optibless: An open-source toolbox for the optimisation of blended stacking sequence, in: 17th European Conference on Composite Materials 2016, European Conference on Composite Materials, ECCM, 2016.
- [101] C. G. Diaconu, M. Sato, H. Sekine, Feasible region in general design space of lamination parameters for laminated composites, *AIAA journal* 40 (3) (2002) 559–565.
- [102] M. M. Abdalla, S. Setoodeh, Z. Gürdal, Design of variable stiffness composite panels for maximum fundamental frequency using lamination parameters, *Composite structures* 81 (2) (2007) 283–291.
- [103] D. Gottlieb, S. A. Orszag, Numerical analysis of spectral methods: theory and applications, SIAM, 1977.
- [104] J. P. Boyd, Chebyshev and Fourier spectral methods, Courier Corporation, 2001.
- [105] B. W. Bader, T. G. Kolda, Algorithm 862: Matlab tensor classes for fast algorithm prototyping, *ACM Transactions on Mathematical Software (TOMS)* 32 (4) (2006) 635–653.
- [106] H. Nguyen-Van, N. Mai-Duy, W. Karunasena, T. Tran-Cong, Buckling and vibration analysis of laminated composite plate/shell structures via a smoothed quadrilateral flat shell element with in-plane rotations, *Computers & structures* 89 (7-8) (2011) 612–625.

- [107] H. An, S. Chen, H. Huang, Multi-objective optimal design of hybrid composite laminates for minimum cost and maximum fundamental frequency and frequency gaps, *Composite Structures* 209 (2019) 268-276.